Spatial and seasonal variations of stable isotope ratios of particulate organic carbon and nitrogen in the surface water of the Kuroshio

KODAMA Taketoshi[1,*]; NISHIMOTO Atsushi[2]; HORII Sachiko[3]; ITO Daiki[1]; YAMAGUCHI Tamaha[1]; HIDAKA Kiyotaka[1]; SETOU Takashi[1]; ONO Tsuneo[1]

[1]Fisheries Resources Institute, Japan Fisheries Research and Education Agency

[2]Fisheries Technology Institute, Japan Fisheries Research and Education Agency

[3]Nagasaki Field Station, Fisheries Resources Institute, Japan Fisheries Research and Education Agency

*Corresponding author

Address: 2-12-4 Fukuura, Kanazawa, Yokohama, Kanagawa 236-8648, Japan

e-mail: takekodama@affrc.go.jp

Running title: Stable isotope ratios of POM in the Kuroshio

Key Points:

- Stable isotope ratios of carbon and nitrogen in particulate organic matter (POM) are seasonally investigated in the vicinity of the Kuroshio
- Generalized linear models show significant seasonality of $\delta^{13}C$ and $\delta^{15}N$ in the POM in coastal and offshore areas
- Atmospheric deposition and nitrogen fixation are contributed to primary production in the summer of the offshore area

Abstract

Stable isotope ratios of carbon and nitrogen ($\delta^{13}C$ and $\delta^{15}N$) in the particulate organic matter (POM) of the euphotic layer were seasonally investigated in the vicinity of the Kuroshio from 2008 to 2019 (n = 490). Generalized linear models (GLMs) showed significant seasonality of $\delta^{13}C$ and $\delta^{15}N$ of POM in the coastal (between Japan Main Island and the northern edge of the Kuroshio) and offshore (Kuroshio and more southern parts) areas. Seasonal climatological $\delta^{13}C$ estimated based on the GLMs and seasonal median values of the environmental parameters was the highest in summer (-22.4 ± 0.2‰ and -22.9 ± 0.2‰ in the coastal and offshore areas, respectively) and lowest in winter in both areas (-23.9 ± 0.2‰ and -24.3 ± 0.2‰ in the coastal and offshore areas, respectively). Seasonal climatological $\delta^{15}N$ showed different spatial variations from spring to summer. The $\delta^{15}N$ value was the lowest during winter (0.8 ± 0.4‰), and increased to a similar level during the other three seasons in the coastal area (~3‰), suggesting that nitrate originating in the deep-sea water was the main source of new production from spring to autumn. In contrast, $\delta^{15}N$ in the offshore areas decreased from spring (2.6 ± 0.4‰) to summer (0.9 ± 0.4‰), suggesting that the significant contributions of atmospheric deposition and nitrogen fixation in the summer were similar to those around Hawaii. Therefore, the nitrogen sources for biological production were different between the areas and seasons in the vicinity of the Kuroshio.

Keywords: Particulate organic matter, Kuroshio, $\delta^{13}C$, $\delta^{15}N$, N_2 fixation, diatoms

1. Introduction

The ocean absorbs large amounts of carbon and nitrogen, which have continuously increased after the industrial revolution [*Archer et al.*, 2009; *Duce et al.*, 2008; *Fowler et al.*, 2013]. To detect the variations of the carbon and nitrogen dynamics in the ocean, the stable isotope ratios of carbon and nitrogen are useful tracers [*Gruber et al.*, 1999; *Keeling*, 1979; *Sigman et al.*, 2009; *Sonnerup et al.*, 1999]. The proportion of ^{13}C to ^{12}C in soluble carbon dioxide in seawater has linearly decreased at a rate of 0.2–0.1‰ decade^{-1} with an increase in the carbon dioxide concentration in the atmosphere [*Gruber et al.*, 1999; *Sonnerup et al.*, 1999]. The long-term linear changes in the ratio of ^{15}N to ^{14}N have been rarely detected in the previous studies of the ocean [*Chiba et al.*, 2012; *Christensen and Richardson*, 2008], but the ratio of ^{15}N to ^{14}N in the coral skeleton-bound organic matter is decreasing with an increase in the anthropogenic nitrogen deposition in this century [*Ren et al.*, 2017].

The Kuroshio is the western boundary current of the North Pacific, and affects the long-term anthropogenic changes in the nitrogen and carbon dynamics [*Ishii et al.*, 2011; *Watanabe et al.*, 2005]. The dynamic also varies seasonally with the physical processes [*Kodama et al.*, 2014b]; the deep convection occurs in winter, while strong stratification occurs in summer. With strong stratification and increase in the surface water temperature, there is an abundance of dinitrogen-fixation cyanobacteria and bacteria in the summer [*Shiozaki et al.*, 2018; *Shiozaki et al.*, 2015]. In addition, water is horizontally transported from the marginal seas and/or the coastal areas to the Kuroshio [*Kodama et al.*, 2015; *Shiozaki et al.*, 2015]. These complex carbon and nitrogen dynamics may support and affect biological productivity in the Kuroshio. The low trophic production in the Kuroshio is one of the most important keys of the fishery resources in Japan and the Pan-Pacific countries. The Kuroshio area is the spawning and nursery

ground for many types of small pelagic fishes, *e.g.* sardine (*Sardinops melanostictus*), and anchovy (*Engraulis japonicus*), in spring [*Ohshimo et al.*, 2019], and migratory tunas, *e.g.* pacific bluefin tuna (*Thunnus orientalis*), yellowfin tuna (*T. albacares*), and skipjack tuna (*Katsuwonus pelamis*), in the summer [*Tanaka et al.*, 2019; *Tawa et al.*, 2020].

The knowledge of the primary production processes in the vicinity of the Kuroshio is limited. In general, determination of the stable isotope ratios of the phytoplankton can be beneficial in understanding the primary production processes. For example, *Mino et al.* [2020] investigated the seasonal variations in the stable isotope ratios of the settling particulate organic matter (POM) collected outside the Kuroshio (station S1: 30°N, 145°E) with sediment traps and reported that the nitrate supplied by deep-sea water accounted for ~90% of the annual new production in this area and the remnant corresponded to the biological nitrogen fixation. A mixture of living and nonliving organic matter exists in the real ocean and it is difficult to separate these [*Volkman and Tanoue*, 2002]; therefore POM, occasionally named seston, is conventionally treated as the proxy of phytoplankton. Stable isotope ratios of the POM are also useful in understanding the grazing food chain, and subsequently the marine ecosystem. The nitrogen isotope ratio of the POM is typically reflected in that of the large predators [*Aita et al.*, 2011; *Horii et al.*, 2018]. *Ohshimo et al.* [2019] determined the carbon and nitrogen isotope ratios in the muscle of the pelagic forage fish and squid in the western North Pacific and reported that their nitrogen isoscape possibly reflected the balance of nitrogen fixation and denitrification, but did not investigate the stable isotope ratios of the POM. In the vicinity of the Kuroshio, fifty-year repeat observations were conducted along 137°E [*Oka et al.*, 2018], but the stable isotope ratios of the marine organisms including those of the POM were not measured in these observations.

Ohshimo et al. [2019] determined both the high and low nitrogen isotope ratios in pelagic forage fish and squid found in the Kuroshio area, and reported that detailed analysis of the stable isotope ratios of the POM were necessary for understanding the grazing food chain and marine ecosystem of this area. Therefore, in this study, carbon and nitrogen stable isotope ratios of the POM in the area adjacent to the Kuroshio water are determined in the over decadal seasonal investigations. The seasonal and yearly variations in the stable isotope ratios of the POM are examined using environmental factors and empirical models, followed by the evaluation of the seasonal climatological values of the stable isotope ratios. The goal of this study is to provide insights into the carbon and nitrogen dynamics in the Kuroshio area, in particular, the nitrogen source for the primary production in this area.

2. Materials and methods

2.1. Observation

POM and environmental data were collected from 2008 to 2019 along the 138°E coordinate between 34°30'N and 27°N (named as "O-line") [*Figure 1*] using R/V *Soyo-maru* of Japan Fisheries Research and Education Agency. The Kuroshio usually flows 32–33°N at 138°E; however, after the Kuroshio large meander in 2017, it flows between 30–32°N [*Figure 1*]. As the Kuroshio shows spatial contrast in the biogeochemical conditions between its northern and southern parts [*Kodama et al.*, 2014b], the observation areas were divided as the coastal (>13 nautical miles north to the Kuroshio axis) and offshore (the Kuroshio and southern part of the Kuroshio axis) areas. The position of the Kuroshio axis was defined as the monthly mean values of the position in the Quick Bulletin of Ocean Conditions published by the Japan Coast Guard (www1.kaiho.mlit.go.jp/KANKYO/KAIYO/qboc/index_E.html).

The POM sampling was conducted seasonally from 2008 to 2015, and the observations were limited to the summer (August or September) and winter (January or February) after 2016 *[Figure 1]*. In summary, the observations were conducted at 23 stations in winter, 30 stations in spring (March, April, or May), 28 stations in summer, and 21 stations in autumn (October or November). After measuring the vertical distributions of the photosensitive available radiation (PAR) using a discreate PAR sensor (PRR-800 or INF-300, Biospherical Instruments Inc., San Diego, California, USA), the water samples were collected using the 12-L X-Niskin bottles attached directly to the cable at five different water depths for which the PAR values were 100, 50, 25, 10, and 1% relative to the surface until May 2016. The sampling depth was fixed after May 2016 within the upper 50 m. The vertical profiles of temperature and salinity were measured using a conductivity-temperature-depth (CTD) sensor (SBE9plus, Sea-Bird Scientific, Washington, USA). The discrete samples for determining nutrient and chlorophyll *a* concentrations were obtained using the Niskin bottles attached to the CTD-CMS (Carousel Multisampling System). Vertical resolution of the discrete samples (nutrients and chlorophyll *a* concentrations) was 10 m depth. As the environmental parameters determined using the POM samples were limited, the nearest depth data collected by the CTD-CMS was adopted for the following statistical analysis. The details of the nutrient and chlorophyll *a* analyses were previously reported in the literature [*Kodama et al.*, 2014b]. To treat the common-logarithm transformed values, the nitrate concentration below 0.01 μM was set as 0.01 μM.

Diatom abundance was investigated at a depth of 10 m for some stations. One liter of seawater samples were collected and fixed with glutaraldehyde solution. The carbon amount of the diatom cells was calculated based on the lengths of the major axes and shapes [*Menden-Deuer and Lessard*, 2000]. The number of one of the major dinitrogen fixation cyanobacteria,

137 *Trichodesmium,* was also counted. These were sporadically present regardless of the season and
138 mostly negligible; therefore, these results are not included.

139

140 **2.2. Isotope analysis**

141 To measure the carbon and nitrogen stable isotope ratios of the POM, three liter of
142 seawater samples were filtered using a pre-combusted (450 °C, 6 h) glass fiber filter (Whatman
143 GF/F, Whatman). The amount of seawater was < 3 L in some case when the filtration time was
144 long. After filtration on board, the samples were kept frozen (-30 °C). In the on-land laboratory,
145 the samples were dried in a dry oven (60 °C, overnight) and kept in a desiccator until
146 decarboxylation.

147 Before measuring the isotope ratio, the samples were exposed to HCl fumes for more
148 than two hours to remove the carbonate salt. After drying again in the dry oven, the colored
149 surfaces of the glass filters were scraped off, and their stable isotope ratios were measured using
150 an isotopic ratio mass spectrometer (MAT 252, Thermo Fisher Scientific (Waltham,
151 Massachusetts, USA) till October 2013, and thereafter, using Isoprime 100 (Elementar,
152 Langenselbold, Germany). The stable isotope ratios of carbon and nitrogen were calibrated
153 using the curves obtained with L-alanine during the measurements. The isotopic compositions of
154 carbon ($\delta^{13}C$) and nitrogen ($\delta^{15}N$) are expressed by following equation:

155 $$\delta X = (R_{sample} / R_{standard} - 1.0) \times 1000, \quad (1)$$

156 where X, R_{sample}, and $R_{standard}$ are the target elements (C or N), and the heavy (^{13}C and ^{15}N) to
157 light (^{12}C and ^{14}N) isotope ratios of the sample and standard, respectively. The standards
158 included atmospheric N_2 for nitrogen and Vienna Pee Dee Belemnite for carbon. The precision

159 of the analysis varied with the amounts of carbon and nitrogen and between the spectrometers,
160 but the values were within 0.2‰ for $\delta^{13}C$ and 1‰ for $\delta^{15}N$. Considering the quality of the
161 standards, the $\delta^{13}C$ and $\delta^{15}N$ values of each sample were rounded off to one decimal place.

162 The $\delta^{13}C$ and $\delta^{15}N$ values of the POM were sometimes the outlier values. Therefore, the
163 mean and standard deviations (sd) were calculated for $\delta^{13}C$ and $\delta^{15}N$ values for all the samples,
164 and the samples whose $\delta^{13}C$ or $\delta^{15}N$ values differed by >3 × sd from the mean values were
165 eliminated. This quality control process was performed twice. In addition, the samples for
166 which the $\delta^{13}C$ and $\delta^{15}N$ values were available, but the environmental parameters were not
167 recorded were removed. As a result, 490 samples out of 526 samples were used in the following
168 statistical analyses. The breakdown of seasonality was as follows: the numbers in winter, spring,
169 summer, and autumn were 108, 147, 133, and 102, respectively. Our data was in the
170 supplemental information.

171

172 **2.3. Statistical Analysis**

173 Statistical analysis was conducted using R version 4.0 [*R Core Team*, 2020]. Generalized
174 linear models (GLMs) were applied to assess the variables that predicted the $\delta^{13}C$ and $\delta^{15}N$
175 values for seasonal and yearly variations. GLM is one of the empirical models for understanding
176 the relationships between explanatory variables and response variables. The models are
177 described as follows:

178 $$\delta X \sim N(\mu, \sigma^2) \quad (2)$$

179 $$\delta X \sim \text{glm}[f(Y) + f(A):f(Sea) + f(A) + f(Sea) + T + Sal + \text{log-Chl} + \text{log-Nit} + Dep + K] \quad (3)$$

180 $$\delta X_{10m} \sim \text{glm}[f(Y) + f(A):f(Sea) + f(A) + f(Sea) + T + Sal + \text{log-Chl} + \text{log-Nit} + \text{log-Diat} + K] \quad (4)$$

where N, μ and σ^2 are the normal distribution, mean, and variance, respectively. δX correspond to $\delta^{13}C$ or $\delta^{15}N$, and δX_{10m} refers to the values at a depth of 10 m, at which the phytoplankton community structures are observed. Y, A, Sea, T, Sal, log-Chl, log-Nit, Dep, log-Diat, and K indicate the sampling year, area (coastal or offshore), season (winter, spring, summer, or autumn), temperature, salinity, common-logarithm transformed chlorophyll *a* concentration (abbreviated as log-chlorophyll, except in the equations), common-logarithm transformed nitrate concentration (log-nitrate, except in the equations), sampling depth, common-logarithm transformed carbon amounts of diatoms (log-diatom, except in the equations), and latitude of the Kuroshio axis, respectively. The letter "f" indicates a categorical variable. For the interaction term between the area and seasons, f(A):f(Sea), it was assumed that the intercept of $\delta^{13}C$ or $\delta^{15}N$ is different between the areas. In these analyses, it was assumed that the environmental parameters were linearly correlated to $\delta^{13}C$ or $\delta^{15}N$; hereafter, the model is described as the linear function GLM. The models using the full data (eq. 3) were considered to be more reliable rather than those limited by the 10 m depth (eq. 4), because the latter had only a small number of data sets, which generated bias in the annual and seasonal sampling. Considering the nonlinear relationship between the explanatory variables and $\delta^{13}C$ or $\delta^{15}N$, the following GLMs were also applied to $\delta^{13}C$ or $\delta^{15}N$:

$$\delta X \sim \mathrm{glm}[\mathrm{f(Y)} + \mathrm{f(A)}:\mathrm{f(Sea)} + \mathrm{f(A)} + \mathrm{f(Sea)} + p(\mathrm{T}, 4) + p(\mathrm{Sal}, 4) + p(\text{log-Chl}, 4) + p(\text{log-Nit}, 4) + p(\mathrm{Dep}, 4) + p(\mathrm{K}, 4)] \quad (5)$$

Here, $p(Z, 4)$ denotes the numerical explanatory variables (Z) applied as quartic functions (degree of 4). Quartic function was selected to avoid overfitting. Hereafter, the model described by eq. 5 is named as the quartic function GLM.

The generalized variance inflation factor (GVIF) was calculated using the "car" package [*Fox and Weisberg*, 2018], and the highest GVIF parameters adjusted using the degree of freedom were <10. The explanatory variables and final model descriptions were selected on the basis of the Akaike Information Criterion (AIC). The "emmeans" package [*Lenth*, 2020] was used to calculate the least squares mean (lsmean) values and standard errors of the yearly variations based on the AIC-selected GLMs. The effects of the parameters were visualized using "response.plot2" function in the "biomod2" package [*Thuiller et al.*, 2020].

3. Results

3.1. Seasonality of environmental parameters

The water temperature was the highest in summer but some cold water (<18 °C) was observed in the coastal area at the subsurface [*Figure 2*]. In summer and autumn, less-saline water (<34) was also found in the area [*Figure 2*], which was attributed to the warm coastal water input (>22 °C). Contrary to the coastal areas, warm and high-salinity water was found in the offshore areas. In the offshore area, water was less-saline in summer than that in winter and spring [*Figure 2*]. The chlorophyll *a* concentration in the coastal area increased in the spring, and decreased in summer [*Figure 2*]. In the offshore area, chlorophyll *a* concentrations in the winter and spring were identical. Nitrate concentration was negligible near the surface from spring to autumn in the offshore area and during summer in the coastal area [*Figure 2*]. At the base of the eutrophic layer (1% light depth), the nitrate was not depleted even in summer. The diatom abundance at a depth of 10 m was the highest during the spring in the coastal area, and it was higher than that of the offshore area during all seasons [*Figure 2*]. In the offshore area, the diatom abundance was identical in winter and spring, but decreased in summer and autumn.

3.2. Isotope ratios

The $\delta^{13}C$ and $\delta^{15}N$ values of POM varied between -28.7 and -20.3‰ for $\delta^{13}C$ and between -4.0 and 8.0‰ for $\delta^{15}N$ (n = 490) [*Figure 3*]. When the data was divided into the area and season, the seasonal variations of both $\delta^{13}C$ and $\delta^{15}N$ values were significant for both the coastal and offshore areas (ANOVA, $p < 0.01$). The 95% probability ellipses showed that both the $\delta^{13}C$ and $\delta^{15}N$ values varied most widely during spring in the coastal area, and those in summer and autumn were within the variations observed during spring [*Figure 3*]. During winter in the coastal area, $\delta^{13}C$ was within the range observed in the spring, but $\delta^{15}N$ was slightly lower. In the offshore area, both $\delta^{13}C$ and $\delta^{15}N$ values varied most widely in the summer, and those during autumn were within the ranges observed in summer. The $\delta^{13}C$ and $\delta^{15}N$ values in winter and spring were slightly lower and higher, respectively, in comparison to those during summer.

3.3. Relationship between environmental parameters and isotope ratios

Significant (F-test, $p<0.05$) linear relationships between $\delta^{13}C$ and several environmental factors, *i.e.* temperature, salinity, and log-nitrate were observed [*Figure 4*]. The coefficients and intercept of the linear regression between $\delta^{13}C$ and temperature were 0.060 ± 0.013 (‰°C^{-1}) and -25.3 ± 0.3‰, respectively, and those between $\delta^{13}C$ and salinity were -2.1 ± 0.20 (‰) and 48.7 ± 6.6‰, respectively. The coefficient of determination (r^2) shows salinity was the strongest explanatory parameter (r^2 = 0.197), and temperature and log-nitrate were weak parameters (r^2 = 0.037 and 0.026, respectively). There was no significant relationship between $\delta^{13}C$ and log-

248 chlorophyll ($p > 0.2$), and the latitude of the Kuroshio axis [*Figure 4*]. There was a positive
249 relationship between $\delta^{13}C$ and log-diatom [*Figure 4*].

250 Significant (*F*-test, $p < 0.05$) linear relationships were observed between $\delta^{15}N$ and both
251 salinity and log-nitrate [*Figure 5*], but both relationships were weak based on the coefficients of
252 determination ($r^2 = 0.008$ and 0.02 for salinity and log-nitrate, respectively). Significant linear
253 relationships were not observed between $\delta^{15}N$ and other environmental factors such as
254 temperature, log-chlorophyll, latitude of Kuroshio axis, and log-diatom. The $\delta^{15}N$ value of the
255 POM increased with an increase in the temperature below 20 °C, but in warm water, the linear
256 trend was not significant [*Figure 5*].

257

258 **3.4. Results of GLMs**

259 The descriptions of the least-AIC GLMs are included in *Table 1.* The sampling depth
260 was selected neither for $\delta^{13}C$ nor $\delta^{15}N$ in all the models. The selected parameters were different
261 in each model, and for $\delta^{15}N$ of the full data model with linear function, only temperature was
262 selected as the environmental parameter. Seasonal and spatial differences including their
263 interaction term were selected in the linear function models, while their interaction term was not
264 included in the quartic function models. The coefficient of determination of the GLMs using the
265 quartic function was higher than those using the linear functions. Yearly variation was not
266 selected only in the model of $\delta^{13}C$ at 10-m depth.

267 The responses of the numerical explanatory variables in the least-AIC GLMs are shown
268 in *Figure 6.* In the full data set model using only the linear functions for $\delta^{13}C$, the negative
269 effects to $\delta^{13}C$ were observed for temperature, salinity, log-nitrate, and latitude of the Kuroshio

axis, while the positive effect was observed for log-chlorophyll [*Figure 6*]. These relationships were statistically significant, except for log-nitrate ($p < 0.05$). In the full data set model considering the nonlinear effects for $\delta^{13}C$, the effect of the latitude of the Kuroshio axis was different from that with the linear function: $\delta^{13}C$ showed higher values when the large mender occurred [*Figure 6*]. The responses of the other parameters were not considerably different from those of the linear functions [*Figure 6*]. The GLM for $\delta^{13}C$ at 10 m depth showed that log-diatom significantly and positively affected the $\delta^{13}C$ values [*Figure 6*].

For $\delta^{15}N$, only temperature was selected and found to positively affect $\delta^{15}N$ in the GLM employing linear functions, while temperature, salinity, log-chlorophyll, and log-nitrate were selected in the GLM including the quartic functions [*Figure 7*]. The temperature showed a unimodal distribution, and the peak of the response was observed at ~20 °C [*Figure 7*]. The unimodal distribution was also observed for log-nitrate; the $\delta^{15}N$ value decreased when the nitrate concentration was greater than the sub-micromolar levels [*Figure 7*]. The increases in log-chlorophyll and salinity showed negative effects on $\delta^{15}N$ [*Figure 7*]. Log-diatom was selected and showed negative effects on $\delta^{15}N$ [*Figure 7*], but the coefficient was not significantly different from 0.

After considering the environmental parameters, spatial, yearly, and seasonal differences were still significant, except the spatial difference of $\delta^{13}C$ estimated from the quartic function-GLM [*Table 1*]. After calculating the yearly lsmean $\delta^{13}C$ and $\delta^{15}N$ values, the reduced sampling frequency after 2017 resulted in large standard errors in $\delta^{13}C$ and $\delta^{15}N$, which made the yearly lsmean values unreliable [*Figure 8*]. In addition, the effects of the Kuroshio large mender after 2018 [*Figure 1*] also made the lsmean $\delta^{13}C$ unreliable, in particular, for the values based on the quartic function GLM [*Figure 8*]. Except these unreliable yearly values (*i.e.* after 2017), lsmean

293 (± SE) $\delta^{13}C$ values ranged between -25.2 ± 0.1‰ (2013) and -23.4 ± 0.2‰ (2008) for the linear
294 function GLM, and between -24.9 ± 0.2‰ (2013) and -23.6 ± 0.2‰ (2008) for the quartic
295 function GLM. In contrast to $\delta^{13}C$, $\delta^{15}N$ varied between 0.6 ± 0.2‰ (2013) and 3.1 ± 0.2‰
296 (2014) for the linear function GLM, and between 2.0 ± 0.3‰ (2013) 4.2 ± 0.3‰ (2014) for the
297 quartic function GLM. In 2013, both the lsmean values of $\delta^{13}C$ and $\delta^{15}N$ were the lowest. The
298 $\delta^{13}C$ and $\delta^{15}N$ values had no significant linear relationships to the year when the data after 2017
299 were removed.

300 For the calculation of the seasonal and spatial lsmean values, the environmental
301 parameters except season and area were fixed. However, in the observations, the environmental
302 parameters showed some degrees of collinearity to the season and/or areas. Therefore, the
303 seasonal and spatial "climatological" $\delta^{13}C$ and $\delta^{15}N$ values were calculated using the least-AIC
304 GLMs and median values of the environmental parameters of each season and area. The year
305 was fixed as 2012, when both the lsmean $\delta^{13}C$ and $\delta^{15}N$ values were neither maximum nor
306 minimum. As a result, significant spatial difference in the seasonality of $\delta^{13}C$ and $\delta^{15}N$ was
307 detected regardless of the linear and quartic function GLMs [*Figure 9*]. Because the coefficients
308 of determination (r^2 values) were greater for the quartic function GLM than those for the linear
309 function GLM [*Table 1*], the numerical values hereafter correspond to the results of the quartic
310 function GLM. In the coastal area, both the climatological $\delta^{13}C$ and $\delta^{15}N$ values were the lowest
311 in winter (-23.9 ± 0.2‰ [mean ± SE] and 0.8 ± 0.4‰, respectively). The $\delta^{15}N$ values were
312 higher than 2.5‰ and similar in the other three seasons (2.7 ± 0.4, 2.7 ± 0.4 and 3.2 ± 0.4‰ in
313 spring, summer, and autumn, respectively). The $\delta^{13}C$ values were highest in summer (-22.4 ±
314 0.2‰), and those during spring and autumn were similar (-23.1 ± 0.2 and -23.2 ± 0.2,
315 respectively). In the offshore area, the seasonal $\delta^{13}C$ and $\delta^{15}N$ values varied in a narrower range

316 than those in the coastal area. The $\delta^{13}C$ values were lowest in winter (-24.3 ± 0.2‰) and highest
317 in summer (-22.9 ± 0.2‰), corresponding to the same trend observed in the coastal area.
318 However, the $\delta^{15}N$ value was the highest in spring (2.6 ± 0.4‰) and lowest in summer (0.9 ±
319 0.4‰). Moreover, the $\delta^{15}N$ value in the offshore area during winter (1.6 ± 0.4‰) was higher
320 than that in the coastal area.

321

322 **4. Discussion**

323 **4.1. Comparison of the previous studies**

324 In the upstream of the Kuroshio and the East China Sea, the horizontal gradients of $\delta^{13}C$
325 and $\delta^{15}N$ of the POM were reported [*Wu et al.*, 2003] to range from -19 to -31‰ for $\delta^{13}C$ and
326 from 0.7 to 9.5‰ for $\delta^{15}N$ in autumn. *Saino and Hattori* [1987] reported only the $\delta^{15}N$ value in
327 the Philippine Sea (western North Pacific Subtropical Gyre), i.e., -1.1‰ at the surface, and
328 *Minagawa et al.* [2001] reported values between -21.6 and -24.4‰ for $\delta^{13}C$ and between ~1‰
329 and ~4‰ for $\delta^{15}N$ in the East China Sea during summer. *Takai et al.* [2007] reported the $\delta^{13}C$
330 and $\delta^{15}N$ values of the POM ranging from -24.2 to -19.1 and 0.7 to 6.8, respectively, around the
331 Izu Peninsula, corresponding to the coastal area of our study but including the ashore area. *Mino*
332 *et al.* [2020] also reported the seasonal variations in the northern edge of the western North
333 Pacific Subtropical Gyre. In their observations, the $\delta^{15}N$ values of the POM ranged between 1.5
334 and 2.6‰ at 0–100 m depth [*Mino et al.*, 2020], but *Mino et al.* [2020] did not report the $\delta^{13}C$
335 values. The ranges for these values are consistent with the results presented herein. Therefore,
336 considering that results in the present study are based on the over-decadal seasonal repeated
337 observations, the climatological $\delta^{15}N$ and $\delta^{13}C$ values herein [*Figure 9*] can be treated as the

338 seasonal climatological values in the Kuroshio area, the western boundary current of the North
339 Pacific.

340 The yearly variations in this study did not show any significant long-term trends for both
341 $\delta^{13}C$ and $\delta^{15}N$ [*Figure 8*]. This was different from the previous studies that inferred the values
342 from the $\delta^{13}C$ content of the fish muscles [*Lorrain et al.*, 2020], which suggested that the $\delta^{13}C$
343 content of the POM decreased linearly in the 21st century. The study period in the present
344 investigation is shorter than the previous studies [*Lorrain et al.*, 2020], and decadal variations of
345 biogeochemical processes are pointed in the Kuroshio [*Oka et al.*, 2019; *Watanabe et al.*, 2005].
346 Therefore, further long-term monitoring of $\delta^{13}C$ and $\delta^{15}N$ is necessary for understanding their
347 variation trends in the POM, and for determining the anthropogenic effects of carbon and
348 nitrogen dynamics in the Kuroshio.

349

350 **4.2. Carbon dynamics in the vicinity of the Kuroshio**

351 Both $\delta^{13}C$ and $\delta^{15}N$ values of the POM are different from those of the phytoplankton
352 because POM contains heterotrophic small planktons and detritus, but it is considered that $\delta^{13}C$
353 and $\delta^{15}N$ values of POM are largely dependent on those of the phytoplankton in open water. The
354 $\delta^{13}C$ value of the phytoplankton depends on the CO_2 concentration in water, growth rate, and cell
355 geometry of each species [*Popp et al.*, 1998]. The growth rate of the phytoplankton depends on
356 temperature, nutrient concentration, and light conditions [*Cross et al.*, 2015], and CO_2
357 concentration in water depends on the temperature, atmospheric CO_2 concentration, and
358 phytoplankton growth. As the result, the $\delta^{13}C$ value of the POM or phytoplankton becomes

359 higher with an increase in the temperature [*Goericke and Fry*, 1994; *Wada et al.*, 2012], and with
360 the rapid growth of the phytoplankton [*Laws et al.*, 1995].

361 However, the $\delta^{13}C$ response to temperature was weak or negligible in the present study
362 contrary to that observed in the previous studies [*Figures 4 and 6*]. The coefficient of simple
363 linear regression analysis between temperature and $\delta^{13}C$ [*Figure 4*] was 0.06 ± 0.01 (‰ $°C^{-1}$),
364 which was smaller than that obtained by the global data estimation (0.17 ± 0.04) [*Goericke and*
365 *Fry*, 1994] and in western North Pacific (0.25) [*Wada et al.*, 2012]. The seasonal variations
366 indicated that the $\delta^{13}C$ value of the POM was high in warm water (for example, $\delta^{13}C$ in the
367 offshore area during summer), but the other factors such as salinity and chlorophyll *a*
368 concentration more significantly affected the $\delta^{13}C$ variations in the Kuroshio. The other possible
369 mechanism for the weak or negligible temperature response was the gravitational downward flux
370 of the POM from the warm surface water to cold subsurface water. When the downward flux
371 was active and heterogenous both in time and space, the relationship between $\delta^{13}C$ and *in situ*
372 temperature was weaker than the empirical values, because the high $\delta^{13}C$ of the POM produced
373 in the warm surface layer was mixed with the low $\delta^{13}C$ of POM produced in the cold subsurface
374 layer.

375 The highest $\delta^{13}C$ value was observed during spring in the coastal area, with a high diatom
376 carbon abundance. The carbon isotopic fractionation of the diatoms is larger than that of the
377 cyanobacteria [*Popp et al.*, 1998]. Therefore, it was considered that rapid growth of diatoms in
378 the blooms afforded the highest $\delta^{13}C$ in the POM during spring in the coastal area. In the coastal
379 area of the Kuroshio, nutrient supply during winter was significantly higher than that in the
380 offshore area [*Kodama et al.*, 2014b]. Thus, the more diatom blooms were observed compared
381 to those in the offshore area, and the $\delta^{13}C$ value of the POM in the coastal area was higher than

382 that in the offshore. The positive coefficient of log-chlorophyll for $\delta^{13}C$ in the GLM also
383 supported that $\delta^{13}C$ of POM elevates during the rapid phytoplankton growth. These observations
384 suggested that carbon sequestration during spring in the coastal area was active, and $\delta^{13}C$ of
385 POM varied with the phytoplankton community structure in the real ocean.

386 The salinity decreased during summer and autumn in the coastal area and showed a
387 negative effect on $\delta^{13}C$ [*Figures 4 and 6*]. Thus, a high $\delta^{13}C$ was observed in less-saline water
388 supply. In the estuary, the $\delta^{13}C$ value of the POM is sometimes affected by the riverine POM
389 [*Bănaru et al.*, 2014]. The intercept of the simple linear relationship between salinity and $\delta^{13}C$
390 indicated that the $\delta^{13}C$ value of the POM in original freshwater was 48.7 ± 6.6‰ if the
391 relationship between salinity and $\delta^{13}C$ was established only based on the results of mixing
392 riverine and oceanic POM. This estimated value was unrealistic: the $\delta^{13}C$ of the riverine POM
393 was between -29.1‰ and -28.7‰ [*Nagao et al.*, 2013; *Nagao et al.*, 2010], between -12‰ and -
394 28‰ at the Ise bay, which was near the observation area of the present study [*Sugimoto et al.*,
395 2004], and -26.9 ± 1.1‰ in the Tokyo bay [*Ogawa and Ogura*, 1997]. Therefore, the high $\delta^{13}C$
396 of the POM in the summer was not the result of the horizontal advective transport of the riverine
397 POM.

398 In addition to the POM, inorganic nutrients are also supplied by the riverine freshwater.
399 With these nutrients, the high $\delta^{13}C$ values of the POM in the estuary reported by the previous
400 studies [*Ogawa and Ogura*, 1997; *Sugimoto et al.*, 2004] are due to the phytoplankton blooms
401 (rapid growth) in the low-salinity nutrient-rich water. With low-salinity water, such a high-$\delta^{13}C$
402 POM is possibly advected from the estuary or eutrophic ashore areas to the investigated area in
403 the present study. In fact, a high $\delta^{13}C$ was observed in the ashore area near this investigated area

404 by *Takai et al.* [2007]. Therefore, considering the $\delta^{13}C$ values, the contribution of the riverine
405 inorganic nutrients may be significant to the productivity in the coastal area of the Kuroshio.

406 The Kuroshio path also affected to $\delta^{13}C$ value of the POM in the GLMs [*Figure 6*]. The
407 coefficients of the linear function GLM suggested that when the Kuroshio flowed near the coast,
408 the $\delta^{13}C$ value of the POM decreased, and when the Kuroshio large meander occurred, the $\delta^{13}C$
409 value of the POM increased. The quartic function GLM indicated that the $\delta^{13}C$ value of the
410 POM was significantly higher when the Kuroshio large meander occurred, but considering the
411 yearly lsmean, the response to the Kuroshio path in the quartic function GLM was unreliable and
412 overfitted. Additional studies are necessary to understand the relationship between the Kuroshio
413 path and $\delta^{13}C$.

414

415 **4.3. Nitrogen dynamics in the vicinity of the Kuroshio**

416 The $\delta^{15}N$ value of the POM varies with $\delta^{15}N$ of the original nitrogen sources (nitrate,
417 ammonium, and N_2 fixation), and degree of isotopic fractionation. The rate of isotopic
418 fractionation of the phytoplankton is controlled by its growth rate [*Wada and Hattori*, 1990].
419 The highest $\delta^{15}N$ value of the POM is produced under nitrate-depleted condition, in which the
420 nitrogen isotopic fractionation of nitrate does not occur [*Wada et al.*, 2012]. The lowest $\delta^{15}N$
421 value of the phytoplankton originates from nitrogen fixation [*Minagawa and Wada*, 1986]. The
422 $\delta^{15}N$ value of the nitrate is 3–5‰ in the vicinity of the Kuroshio [*Sugimoto et al.*, 2009;
423 *Yoshikawa et al.*, 2018]. In winter, vertical mixing occurs, and nitrate is present at a micromolar
424 level both in the coastal and offshore areas in the euphotic layer [*Figure 2*]. In spring,
425 stratification starts occurring, and the nitrate in the offshore depletes but is detectable at the sub-

426 micromolar level [*Figure 2*]. The $\delta^{15}N$ value of the POM (phytoplankton) is lower than that of
427 the nitrate under conditions with sufficient nitrate [*Fogel and Cifuentes*, 1993; *Montoya and*
428 *McCarthy*, 1995; *Wada*, 1980]. Therefore, the lower climatological $\delta^{15}N$ values of the POM in
429 winter (0.8 ± 0.4 and 1.6 ± 0.4‰ in the coastal and offshore areas, respectively, Figure 9)
430 compared to those during spring were owing to the difference in the nitrate, *i.e.*, nitrate
431 consumption was lower than nitrate supply in the winter, while nitrate consumption was greater
432 than nitrate supply in the spring. Similar phenomenon was reported by *Mino et al.* [2020]. The
433 $\delta^{15}N$ value of the POM in the sediment traps [*Mino et al.*, 2020] was higher than the values in
434 water, but a decrease in the $\delta^{15}N$ value of the POM in the winter was similar because of the
435 active nitrate supply due to deep mixing.

436 During summer, nitrate was largely depleted both in the coastal and offshore areas at the
437 surface, but still remained at the base of the euphotic layer in the coastal area [*Figure 2*]. In
438 addition, ammonium was depleted in the offshore area, while it remained in the coastal area at
439 the nanomolar level [*Kodama et al.*, 2014a], and nitracline was shallower in the coastal area than
440 in the offshore area [*Kodama et al.*, 2014b]. These observations suggested that the nitrate-
441 originating new production was active in the coastal waters, but not in the offshore water.

442 Two possible sources that decrease $\delta^{15}N$ of the POM in the offshore area during summer
443 are 1) nitrogen fixation and 2) wet and dry deposition of the nitrogenous nutrients from the
444 atmosphere. First, the Kuroshio and western North Pacific are two of the "hotspots" of nitrogen
445 fixation during summer [*Shiozaki et al.*, 2010; *Shiozaki et al.*, 2018; *Shiozaki et al.*, 2015]. In the
446 microscopic observations at 10 m depth, *Trichodesmium* is not abundant but an important
447 dinitrogen-fixation phytoplankton in the Kuroshio [*Shiozaki et al.*, 2018; *Shiozaki et al.*, 2015],
448 which floats upward and accumulates at the surface [*Walsby*, 1992]. The $\delta^{15}N$ of *Trichodesmium*

449 ranges between -2.1 and 0.8‰ [*Minagawa and Wada*, 1986]. Therefore, the decrease in $\delta^{15}N$ of
450 the POM during the winter was attributed to active nitrogen fixation.

451 Second, the wet and dry deposition of nitrogenous nutrient inputs from nitrogen fixation
452 and nitrate supply from deep water in the upstream of the Kuroshio are similar during summer
453 [*Kodama et al.*, 2011], and $\delta^{15}N$ of the nitrate in rainwater is <0‰ in Japan [*Wu et al.*, 2008].
454 Therefore, the wet and dry deposition of nitrogenous nutrient inputs also decrease the $\delta^{15}N$ of the
455 POM. Both factors decreased the $\delta^{15}N$ of the POM in the offshore area during summer. In the
456 autumn, the mixing layer deepened, and the nitrate concentration again increased in the euphotic
457 layer [*Figure 2*], and thus, $\delta^{15}N$ value of the POM was a mixture of the summer values and
458 nitrate-originating values.

459 In the coastal area, the climatological $\delta^{15}N$ value in the summer was similar to that during
460 spring, suggesting that the contributions of nitrogen fixation and atmospheric deposition were
461 small during the summer. In contrast, salinity decreased in the summer; therefore, riverine
462 inputs as well as nitrogen fixation and atmospheric depositions must be considered because
463 riverine inputs of the nitrogenous nutrients possibly comprise ~10% of the nitrogenous nutrient
464 input in the coastal area [*Kodama et al.*, 2014b]. The aforementioned relationship between
465 salinity and $\delta^{13}C$ also indicated that riverine inputs of the nitrogenous nutrients influenced the
466 productivity in the coastal area. However, the $\delta^{15}N$ value of riverine nitrate varied from 0 to 8‰,
467 and decreased with an increase in the river discharge and was unstable [*Sugimoto et al.*, 2011].
468 The $\delta^{15}N$ of ammonium was high (typically >10‰), but the concentration of ammonium was
469 approximately one-third of nitrate in the river discharge [*Sugimoto et al.*, 2011]. Therefore, the
470 impact of riverine water on the $\delta^{15}N$ value of the POM was not evaluated in this study.

As nitrogen fixation and atmospheric deposition decreased the $\delta^{15}N$ value of the POM in the offshore area, the contributions of these nitrogenous inputs were estimated. Assuming that all $\delta^{15}N$ in the POM originating from nitrogen fixation, atmospheric deposition, and ammonium was -1‰ [*Knapp et al.*, 2011; *Minagawa and Wada*, 1986; *Wu et al.*, 2008] and that from deep-sea nitrate was 4‰ based on $\delta^{15}N$ of the nitrate [*Mino et al.*, 2020; *Sugimoto et al.*, 2009; *Yoshikawa et al.*, 2018], the deep-sea nitrate-originating POM comprised only one-third of the average POM (36%) in the offshore area during summer ($\delta^{15}N$ is 0.8‰). This estimated contribution of the deep-sea nitrate-originating POM was possibly an overestimation because the contributions of the dissolved organic nitrogen (DON), whose $\delta^{15}N$ was high, as well as that of nitrate, were ignored [*Knapp et al.*, 2011]. In other seasons, nitrate concentration was often detectable; thus, the isotopic fraction during nitrate assimilation was not ignored, and the contribution of deep-sea nitrate must be underestimated in our calculations.

The source of new nitrogen is more appropriately estimated based on the $\delta^{15}N$ value of the sinking POM [*Casciotti et al.*, 2008]. At station ALOHA set off Hawaii, the annual mean contribution of nitrogen fixation is 26–69% of the exported POM [*Böttjer et al.*, 2017; *Casciotti et al.*, 2008; *Dore et al.*, 2002]. At station S1 set in the western North Pacific, the annual contribution of nitrogen fixation is 7–14% [*Mino et al.*, 2020]. The $\delta^{15}N$ of the POM in the present study during summer was similar to that measured in the euphotic layer at station ALOHA during summer [*Casciotti et al.*, 2008], slightly lower than that at station S1 [*Mino et al.*, 2020], and higher than that in the western South Pacific Subtropical Gyre [*Shiozaki et al.*, 2014]. Therefore, the contributions of nitrogen fixation and atmospheric deposition to the new production in the Kuroshio area during summer and at station ALOHA are significant, but these are not lower than those in the western South Pacific Subtropical Gyre, and are at least one-

494 quarter of the new production in this area. Considering the yearly lsmean of $\delta^{15}N$, the
495 contribution of deep-sea nitrate varies interannually. For example, its contribution was ~30%
496 lower than the average in 2013 in both the models, but the reason was not clear in this study.
497

498 **5. Conclusion**

499 This study reports the seasonal variations in the $\delta^{13}C$ and $\delta^{15}N$ values of the POM in the
500 euphotic layer based on the middle term (~10 years) repeated seasonal observations. The spatio-
501 seasonal variations in $\delta^{13}C$ and $\delta^{15}N$ of POM show that the primary production in the vicinity of
502 the Kuroshio is supported by many physical and biological processes, i.e., during the nitrate-
503 sufficient and well-mixed conditions in winter, a low $\delta^{15}N$ indicates the dominance of nitrate-
504 originating primary production. When the stratification develops, and nitrate depletes in the
505 spring, a high $\delta^{15}N$ suggests that the isotopic fractionation of nitrate does not occur. In the
506 summer, diazotrophs and atmospheric deposition play important roles in the primary production
507 in the offshore area, while contribution from deep-sea nitrate remains active in the coastal area;
508 the contribution of riverine nitrogenous nutrient is considered significant, but cannot be
509 evaluated based on $\delta^{15}N$. The deep-sea nitrate-originating production is considered to be limited
510 to one-third of primary production in the offshore area during summer. The carbon dynamics
511 also exhibit spatio-seasonality. In the coastal area, the spring diatom blooms result in high $\delta^{13}C$-
512 POM, whereas in the offshore, high $\delta^{13}C$-POM is formed in the summer. High $\delta^{13}C$-POM is also
513 present in low-salinity water in the coastal area, which may be caused by the horizontal
514 advection of the ashore water, and significantly affects the primary production in the coastal
515 area. Therefore, complex biogeochemical processes support the primary production in the
516 vicinity of the Kuroshio and the subsequent fishery production in the Pacific.

517 The yearly variation of the lsmean $\delta^{15}N$ indicates that the proportion of deep-sea nitrate
518 and nitrogen fixation or atmospheric deposition for the new production is not homogenous.
519 However, the yearly linear trends and the effect of the Kuroshio large mender are not clearly
520 observed because the Kuroshio large mender occurred after 2018; recent changes in the $\delta^{15}N$ and
521 $\delta^{13}C$ values of the POM are not sufficient to elucidate the effects. As the Kuroshio path shows a
522 large impact on the ecosystems in the Kuroshio [*Hiraoka et al.*, 2019; *Nakata et al.*, 2000],
523 further studies are necessary to understand the yearly variations and anthropogenic impact on the
524 primary production of the Kuroshio area.
525

Acknowledgement

We thank the captains, officers, crew members, and scientists of the R/V *Soyo-maru* cruise for their cooperation at the sea. We are grateful to K. Yamada and T. Ichikawa for analyses and providing data. E. Wada and S. Ohshimo kindly commented on an earlier draft of the manuscript. Our data is published as the supplemental information of this article. This study was financially supported by Fisheries Agency, Japan Fisheries Research and Education Agency, Agriculture, Forestry and Fisheries Research Council through a research project entitled "Development of Technologies for Mitigation and Adaptation to Climate Change in Agriculture, Forestry and Fisheries", and JSPS KAKENHI Grant Numbers 19K06198 (to TK), 19H03038 (to KH, TY, and TI), and 19K24396 (to TY).

537 **Table 1**. Descriptions of the least Akaike Information Criterion generalized linear models (AIC GLMs)

538 and their coefficients of determination (r^2). The abbreviations are the same as those described in eq. 3.

	Least AIC models	r^2
Linear function		
$\delta^{13}C$	f(Y) + f(A):f(Sea) + f(A) + f(Sea) + T + Sal + log-chl + log-nit + K	0.443
$\delta^{15}N$	f(Y) + f(A):f(Sea) + T	0.309
Quartic function		
$\delta^{13}C$	f(Y) + f(Sea) + *p*(T) + *p*(Sal) + *p*(log-chl) + *p*(log-nit) + *p*(K)	0.596
$\delta^{15}N$	f(Y) + f(A) + f(Sea) + *p*(T) + *p*(Sal) + *p*(log-chl) + *p*(log-nit)	0.387
Linear function including diatom abundance (10 m depth only)		
$\delta^{13}C_{10\ m}$	f(A) +f(Sea) + Sal + log-Chl + log-Nit + log-Diat + K	0.817
$\delta^{15}N_{10\ m}$	f(Y) + f(A):f(Sea) + f(A) + f(Sea) + T + log-Chl + log-Nit + log-Diat	0.659

539

References

Aita, M. N., K. Tadokoro, N. O. Ogawa, F. Hyodo, R. Ishii, S. L. Smith, T. Saino, M. J. Kishi, S.-I. Saitoh, and E. Wada (2011), Linear relationship between carbon and nitrogen isotope ratios along simple food chains in marine environments, *J. Plankton Res.*, *33*(11), 1629-1642, doi:10.1093/plankt/fbr070.

Archer, D., et al. (2009), Atmospheric lifetime of fossil fuel carbon dioxide, *Annu. Rev. Earth Planet. Sci.*, *37*(1), 117-134, doi:10.1146/annurev.earth.031208.100206.

Bănaru, D., F. Carlotti, A. Barani, G. Grégori, N. Neffati, and M. Harmelin-Vivien (2014), Seasonal variation of stable isotope ratios of size-fractionated zooplankton in the Bay of Marseille (NW Mediterranean Sea), *J. Plankton Res.*, *36*(1), 145-156, doi:10.1093/plankt/fbt083.

Böttjer, D., J. E. Dore, D. M. Karl, R. M. Letelier, C. Mahaffey, S. T. Wilson, J. Zehr, and M. J. Church (2017), Temporal variability of nitrogen fixation and particulate nitrogen export at Station ALOHA, *Limnol. Oceanogr.*, *62*(1), 200-216, doi:10.1002/lno.10386.

Casciotti, K. L., T. W. Trull, D. M. Glover, and D. Davies (2008), Constraints on nitrogen cycling at the subtropical North Pacific Station ALOHA from isotopic measurements of nitrate and particulate nitrogen, *Deep Sea Res. II*, *55*(14), 1661-1672, doi:10.1016/j.dsr2.2008.04.017.

Chiba, S., H. Sugisaki, A. Kuwata, K. Tadokoro, T. Kobari, A. Yamaguchi, and D. L. Mackas (2012), Pan-North Pacific comparison of long-term variation in Neocalanus copepods based on stable isotope analysis, *Prog. Oceanogr.*, *97-100*, 63-75, doi:10.1016/j.pocean.2011.11.007.

Christensen, J. T., and K. Richardson (2008), Stable isotope evidence of long-term changes in the North Sea food web structure, *Mar. Ecol. Prog. Ser.*, *368*, 1-8, doi:10.3354/meps07635.

Cross, W. F., J. M. Hood, J. P. Benstead, A. D. Huryn, and D. Nelson (2015), Interactions between temperature and nutrients across levels of ecological organization, *Glob Chang Biol*, *21*(3), 1025-1040, doi:10.1111/gcb.12809.

Dore, J. E., J. R. Brum, L. M. Tupas, and D. M. Karl (2002), Seasonal and interannual variability in sources of nitrogen supporting export in the oligotrophic subtropical North Pacific Ocean, *Limnol. Oceanogr.*, *47*(6), 1595-1607, doi:10.4319/lo.2002.47.6.1595.

Duce, R. A., et al. (2008), Impacts of atmospheric anthropogenic nitrogen on the open ocean, *Science*, *320*(5878), 893-897, doi:10.1126/science.1150369.

Fogel, M. L., and L. A. Cifuentes (1993), Isotope fractionation during primary production, in *Org. Geochem.*, edited by M. H. Engel and S. A. Macko, pp. 73-98, Springer US, Boston, MA, doi:10.1007/978-1-4615-2890-6_3.

Fowler, D., M. Coyle, U. Skiba, M. A. Sutton, J. N. Cape, S. Reis, L. J. Sheppard, A. Jenkins, B. Grizzetti, and J. N. Galloway (2013), The global nitrogen cycle in the twenty-first century, *Philos. T. R. Soc. B*, *368*(1621), 20130164, doi:10.1098/rstb.2013.0164.

575 Fox, J., and S. Weisberg (2018), *An R companion to applied regression*, Sage publications.

576 Goericke, R., and B. Fry (1994), Variations of marine plankton δ13C with latitude, temperature, and
577 dissolved CO2 in the world ocean, *Global Biogeochem. Cycles*, *8*(1), 85-90,
578 doi:10.1029/93gb03272.

579 Gruber, N., C. D. Keeling, R. B. Bacastow, P. R. Guenther, T. J. Lueker, M. Wahlen, H. A. J. Meijer, W.
580 G. Mook, and T. F. Stocker (1999), Spatiotemporal patterns of carbon-13 in the global surface
581 oceans and the oceanic suess effect, *Global Biogeochem. Cycles*, *13*(2), 307-335,
582 doi:10.1029/1999gb900019.

583 Hiraoka, Y., K. Fujioka, H. Fukuda, M. Watai, and S. Ohshimo (2019), Interannual variation of the diet
584 shifts and their effects on the fatness and growth of age-0 Pacific bluefin tuna (*Thunnus*
585 *orientalis*) off the southwestern Pacific coast of Japan, *Fish. Oceanogr.*, *28*(4), 419-433,
586 doi:10.1111/fog.12421.

587 Horii, S., K. Takahashi, T. Shiozaki, F. Hashihama, and K. Furuya (2018), Stable isotopic evidence for the
588 differential contribution of diazotrophs to the epipelagic grazing food chain in the mid-Pacific
589 Ocean, *Global Ecol. Biogeogr.*, *27*(12), 1467-1480, doi:10.1111/geb.12823.

590 Ishii, M., N. Kosugi, D. Sasano, S. Saito, T. Midorikawa, and H. Y. Inoue (2011), Ocean acidification off
591 the south coast of Japan: A result from time series observations of CO2parameters from 1994 to
592 2008, *J. Geophys. Res.*, *116*(C6), doi:10.1029/2010jc006831.

593 Keeling, C. D. (1979), The Suess effect: 13Carbon-14Carbon interrelations, *Environ. Int.*, *2*(4-6), 229-
594 300, doi:10.1016/0160-4120(79)90005-9.

595 Knapp, A. N., D. M. Sigman, F. Lipschultz, A. B. Kustka, and D. G. Capone (2011), Interbasin isotopic
596 correspondence between upper-ocean bulk DON and subsurface nitrate and its implications for
597 marine nitrogen cycling, *Global Biogeochem. Cycles*, *25*(4), doi:10.1029/2010gb003878.

598 Kodama, T., K. Furuya, F. Hashihama, S. Takeda, and J. Kanda (2011), Occurrence of rain-origin nitrate
599 patches at the nutrient-depleted surface in the East China Sea and the Philippine Sea during
600 summer, *J. Geophys. Res.*, *116*(C8), C08003, doi:10.1029/2010jc006814.

601 Kodama, T., T. Ichikawa, K. Hidaka, and K. Furuya (2014a), A highly sensitive and large concentration
602 range colorimetric continuous flow analysis for ammonium concentration, *J. Oceanogr.*, *71*(1),
603 65-75, doi:10.1007/s10872-014-0260-6.

604 Kodama, T., T. Setou, M. Masujima, M. Okazaki, and T. Ichikawa (2015), Intrusions of excess nitrate in
605 the Kuroshio subsurface layer, *Cont. Shelf Res.*, *110*, 191-200, doi:10.1016/j.csr.2015.10.012.

606 Kodama, T., Y. Shimizu, T. Ichikawa, Y. Hiroe, A. Kusaka, H. Morita, M. Shimizu, and K. Hidaka
607 (2014b), Seasonal and spatial contrast in the surface layer nutrient content around the Kuroshio
608 along 138°E, observed between 2002 and 2013, *J. Oceanogr.*, *70*(6), 489-503,
609 doi:10.1007/s10872-014-0245-5.

610 Laws, E. A., B. N. Popp, R. R. Bidigare, M. C. Kennicutt, and S. A. Macko (1995), Dependence of
611 phytoplankton carbon isotopic composition on growth rate and [CO2)aq: Theoretical

612 considerations and experimental results, *Geochim. Cosmochim. Acta*, *59*(6), 1131-1138,
613 doi:10.1016/0016-7037(95)00030-4.

614 Lenth, R. (2020), emmeans: Estimated marginal means, aka least-squares means, edited, https://CRAN.R-
615 project.org/package=emmean.

616 Lorrain, A., et al. (2020), Trends in tuna carbon isotopes suggest global changes in pelagic phytoplankton
617 communities, *Glob Chang Biol*, *26*(2), 458-470, doi:10.1111/gcb.14858.

618 Menden-Deuer, S., and E. J. Lessard (2000), Carbon to volume relationships for dinoflagellates, diatoms,
619 and other protist plankton, *Limnol. Oceanogr.*, *45*(3), 569-579, doi:10.4319/lo.2000.45.3.0569.

620 Minagawa, M., M. Ohashi, T. Kuramoto, and N. Noda (2001), δ15N of PON and nitrate as a clue to the
621 origin and transformation of nitrogen in the subarctic North Pacific and its marginal sea, *J.*
622 *Oceanogr.*, *57*(3), 285-300, doi:10.1023/a:1012430512137.

623 Minagawa, M., and E. Wada (1986), Nitrogen isotope ratios of red tide organisms in the East China Sea:
624 A characterization of biological nitrogen fixation, *Mar. Chem.*, *19*(3), 245-259, doi:10.1016/0304-
625 4203(86)90026-5.

626 Mino, Y., et al. (2020), Seasonal and Interannual Variations in Nitrogen Availability and Particle Export in
627 the Northwestern North Pacific Subtropical Gyre, *J. Geophys. Res.*, *125*(5), e2019JC015600,
628 doi:10.1029/2019jc015600.

629 Montoya, J. P., and J. J. McCarthy (1995), Isotopic fractionation during nitrate uptake by phytoplankton
630 grown in continuous culture, *J. Plankton Res.*, *17*(3), 439-464, doi:10.1093/plankt/17.3.439.

631 Nagao, S., T. Aramaki, N. Fujitake, H. Kodama, T. Tanaka, S. Ochiai, M. Uchida, Y. Shibata, and M.
632 Yamamoto (2013), Variation of Δ14C and δ13C values of dissolved humic and fulvic acids in the
633 Tokachi river system in northern Japan, *Radiocarbon*, *55*(Nr2-3), 1007-1016.

634 Nagao, S., T. Aramaki, O. Seki, M. Uchida, and Y. Shibata (2010), Carbon isotopes and lignin
635 composition of POC in a small river in Bekanbeushi Moor, northern Japan, *Nuclear Instruments*
636 *and Methods in Physics Research Section B: Beam Interactions with Materials and Atoms*, *268*(7-
637 8), 1098-1101, doi:10.1016/j.nimb.2009.10.108.

638 Nakata, H., S. Funakoshi, and M. Nakamura (2000), Alternating dominance of postlarval sardine and
639 anchovy caught by coastal fishery in relation to the Kuroshio meander in the Enshu-nada Sea,
640 *Fish. Oceanogr.*, *9*(3), 248-258, doi:10.1046/j.1365-2419.2000.00140.x.

641 Ogawa, N., and N. Ogura (1997), Dynamics of particulate organic matter in the Tamagawa estuary and
642 inner Tokyo Bay, *Estuar. Coast. Shelf. Sci.*, *44*(3), 263-273, doi:10.1006/ecss.1996.0118.

643 Ohshimo, S., D. J. Madigan, T. Kodama, H. Tanaka, K. Komoto, S. Suyama, T. Ono, and T. Yamakawa
644 (2019), Isoscapes reveal patterns of δ13C and δ15N of pelagic forage fish and squid in the
645 Northwest Pacific Ocean, *Prog. Oceanogr.*, *175*, 124-138, doi:10.1016/j.pocean.2019.04.003.

Oka, E., M. Ishii, T. Nakano, T. Suga, S. Kouketsu, M. Miyamoto, H. Nakano, B. Qiu, S. Sugimoto, and Y. Takatani (2018), Fifty years of the 137°E repeat hydrographic section in the western North Pacific Ocean, *J. Oceanogr.*, *74*(2), 115-145, doi:10.1007/s10872-017-0461-x.

Oka, E., K. Yamada, D. Sasano, K. Enyo, T. Nakano, and M. Ishii (2019), Remotely forced decadal physical and biogeochemical variability of North Pacific Subtropical Mode water over the last 40 years, *Geophys. Res. Lett.*, *46*(3), 1555-1561, doi:10.1029/2018gl081330.

Popp, B. N., E. A. Laws, R. R. Bidigare, J. E. Dore, K. L. Hanson, and S. G. Wakeham (1998), Effect of phytoplankton cell geometry on carbon isotopic fractionation, *Geochim. Cosmochim. Acta*, *62*(1), 69-77, doi:10.1016/s0016-7037(97)00333-5.

R Core Team (2020), R: A language and environment for statistical computing, edited by R Foundation for Statistical Computing, https://www.R-project.org/. Vienna, Austria.

Ren, H., Y. C. Chen, X. T. Wang, G. T. F. Wong, A. L. Cohen, T. M. DeCarlo, M. A. Weigand, H. S. Mii, and D. M. Sigman (2017), 21st-century rise in anthropogenic nitrogen deposition on a remote coral reef, *Science*, *356*(6339), 749-752, doi:10.1126/science.aal3869.

Saino, T., and A. Hattori (1987), Geographical variation of the water column distrubution of suspended particulate organic nitrogen and its 15N natural abundance in the Pacific and its marginal seas, *Deep Sea Res. A*, *34*(5-6), 807-827, doi:10.1016/0198-0149(87)90038-0.

Shiozaki, T., K. Furuya, T. Kodama, S. Kitajima, S. Takeda, T. Takemura, and J. Kanda (2010), New estimation of N2 fixation in the western and central Pacific Ocean and its marginal seas, *Global Biogeochem. Cycles*, *24*(1), GB1015, doi:10.1029/2009gb003620.

Shiozaki, T., T. Kodama, and K. Furuya (2014), Large-scale impact of the island mass effect through nitrogen fixation in the western South Pacific Ocean, *Geophys. Res. Lett.*, *41*(8), 2907-2913, doi:10.1002/2014GL059835.

Shiozaki, T., Y. Kondo, D. Yuasa, and S. Takeda (2018), Distribution of major diazotrophs in the surface water of the Kuroshio from northeastern Taiwan to south of mainland Japan, *J. Plankton Res.*, *40*(4), 407-419, doi:10.1093/plankt/fby027.

Shiozaki, T., S. Takeda, S. Itoh, T. Kodama, X. Liu, F. Hashihama, and K. Furuya (2015), Why is Trichodesmium abundant in the Kuroshio?, *Biogeosciences*, *12*(23), 6931-6943, doi:10.5194/bg-12-6931-2015.

Sigman, D. M., K. L. Karsh, and K. L. Casciotti (2009), Nitrogen isotopes in the ocean, in *Encyclopedia of Ocean Sciences*, edited by J. H. Steele, pp. 40-54, Academic Press, Oxford, doi:10.1016/b978-012374473-9.00632-9.

Sonnerup, R. E., P. D. Quay, A. P. McNichol, J. L. Bullister, T. A. Westby, and H. L. Anderson (1999), Reconstructing the oceanic 13C Suess Effect, *Global Biogeochem. Cycles*, *13*(4), 857-872, doi:10.1029/1999gb900027.

Sugimoto, R., A. Kasai, K. Fujita, K. Sakaguchi, and T. Mizuno (2011), Assessment of nitrogen loading from the Kiso-Sansen Rivers into Ise Bay using stable isotopes, *J. Oceanogr.*, *67*(2), 231-240, doi:10.1007/s10872-011-0022-7.

Sugimoto, R., A. Kasai, T. Miyajima, and K. Fujita (2009), Nitrogen isotope ratios of nitrate as a clue to the origin of nitrogen on the Pacific coast of Japan, *Cont. Shelf Res.*, *29*(10), 1303-1309, doi:10.1016/j.csr.2009.03.007.

Sugimoto, R., A. Kasai, S. Yamao, T. Fujiwara, and T. Kimura (2004), Variation in particulate organic matter accompanying changes of river discharge in Ise Bay, *Bull. Jap. Soc. Fish. Oceanogr.*, *68*(3), 142-150.

Takai, N., N. Hirose, T. Osawa, K. Hagiwara, T. Kojima, Y. Okazaki, T. Kuwae, T. Taniuchi, and K. Yoshihara (2007), Carbon source and trophic position of pelagic fish in coastal waters of south-eastern Izu Peninsula, Japan, identified by stable isotope analysis, *Fish. Sci.*, *73*(3), 593-608, doi:10.1111/j.1444-2906.2007.01372.x.

Tanaka, Y., A. Tawa, T. Ishihara, E. Sawai, M. Nakae, M. Masujima, and T. Kodama (2019), Occurrence of Pacific bluefin tuna *Thunnus orientalis* larvae off the Pacific coast of Tohoku area, northeastern Japan: Possibility of the discovery of the third spawning ground, *Fish. Oceanogr.*, *29*(1), 46-51, doi:10.1111/fog.12445.

Tawa, A., T. Kodama, K. Sakuma, T. Ishihara, and S. Ohshimo (2020), Fine-scale horizontal distributions of multiple species of larval tuna off the Nansei Islands, Japan, *Mar. Ecol. Prog. Ser.*, *636*, 123-137, doi:10.3354/meps13216.

Thuiller, W., D. Georges, R. Engler, and F. Breiner (2020), biomod2: Ensemble Platform for Species Distribution Modeling, edited.

Volkman, J. K., and E. Tanoue (2002), Chemical and biological studies of particulate organic matter in the ocean, *J. Oceanogr.*, *58*(2), 265-279, doi:10.1023/A:1015809708632.

Wada, E. (1980), Nitrogen isotope fractionation and its significance in biogeochemical processes occurring in marine environments, in *Isotope Marine Chemistry*, edited by E. Goldberg, Y. Horibe and K. Saruhashi, pp. 375-398, Uchida Rokakuho, Tokyo.

Wada, E., and A. Hattori (1990), *Nitrogen in the sea: forms, abundance, and rate processes*, CRC press, Florida, USA.

Wada, E., K. Ohki, S. Yoshikawa, P. L. Parker, C. V. Baalen, G. I. Matsumoto, M. N. Aita, and T. Saino (2012), Ecological aspects of carbon and nitrogen isotope ratios of cyanobacteria, *Plank. Benth. Res.*, *7*(3), 135-145, doi:10.3800/pbr.7.135.

Walsby, A. E. (1992), The gas vesicles and buoyancy of *Trichodesmium*, in *Marine Pelagic Cyanobacteria: Trichodesmium and other Diazotrophs*, edited by E. J. Carpenter, D. G. Capone and J. G. Rueter, pp. 141-161, Springer Netherlands, Dordrecht, doi:10.1007/978-94-015-7977-3_9.

717 Watanabe, Y. W., H. Ishida, T. Nakano, and N. Nagai (2005), Spatiotemporal decreases of nutrients and
718 chlorophyll-*a* in the surface mixed layer of the western North Pacific from 1971 to 2000, *J.*
719 *Oceanogr.*, *61*(6), 1011-1016, doi:10.1007/s10872-006-0017-y.

720 Wu, J., Y. Nishijima, and H. Satake (2008), Seasonal variation of δ15N of nitrate ion found in
721 precipitation at Toyama, *Chikyukagaku*, *42*(1), 1-11, doi:10.14934/chikyukagaku.42.1.

722 Wu, Y., J. Zhang, D. J. Li, H. Wei, and R. X. Lu (2003), Isotope variability of particulate organic matter at
723 the PN section in the East China Sea, *Biogeochemistry*, *65*(1), 31-49,
724 doi:10.1023/a:1026044324643.

725 Yoshikawa, C., A. Makabe, Y. Matsui, T. Nunoura, and N. Ohkouchi (2018), Nitrate isotope distribution
726 in the Subarctic and Subtropical North Pacific, *Geochemistry, Geophysics, Geosystems*, *19*(7),
727 2212-2224, doi:10.1029/2018gc007528.

728

729

730 Figure Captions

731 **Figure 1**. (a) Map of the sampling site and depiction of the flow of the Kuroshio current. Light
732 and dark gray lines represent the normal path (January 2015) and large-meandered
733 path of the Kuroshio current (January 2018), respectively. Black line depicts the "O-
734 line". (b) Temporal variations of the sampling stations (circles and squares) and the
735 Kuroshio axis (solid gray line) along the O-line. Light and dark gray boxes in (b)
736 denote the summer and winter periods, respectively. Closed circles and squares
737 correspond to the coastal and offshore stations, respectively.

738 **Figure 2**. Seasonal variations in (a) temperature, (b) salinity, (c) chlorophyll a concentration, (d)
739 nitrate concentration, and (e) carbon-based diatom abundance. Dark blue and green
740 boxes indicate the data in the coastal and offshore areas, respectively. Chlorophyll *a*
741 concentration, nitrate concentration, and carbon-based diatom abundance are
742 converted into common-logarithm values. Each boxplot shows the medians (vertical
743 thick lines within boxes), upper and lower quartiles (boxes), quartile deviations
744 (horizontal bars), and outliers (circles).

745 **Figure 3**. Scatter diagrams for $\delta^{15}N$ and $\delta^{13}C$ of POM along the O-line in the (a) coastal and (b)
746 offshore areas. Circles and crosses indicate the samples collected in the coastal and
747 offshore areas, and the colors denote the different seasons. The ellipses include 95%
748 probability ellipse for each season and area.

749 **Figure 4**. Relationship between $\delta^{13}C$ and (a) temperature, (b) salinity, (c) common-logarithm
750 transformed chlorophyll a concentration (log-chlorophyll), (d) common-logarithm
751 transformed nitrate concentration (log-nitrate), (e) latitude of the Kuroshio axis, and (f)
752 common-logarithm transformed carbon-based diatom abundance (log-diatom).

Diatom abundance data is available at only 10-m depth. The colors and shapes denote the areas and seasons, respectively (blue: coastal; green: offshore; closed circle: winter; open triangle: spring; cross: summer; closed square: autumn). The gray solid dashed line with shadow represents the linear regression line and 95% confidence values. When the linear regression line is the dashed line, the linear regression relationship is not significant ($p > 0.05$).

Figure 5. Relationship between $\delta^{15}N$ and (a) temperature, (b) salinity, (c) common-logarithm transformed chlorophyll a concentration (log-chlorophyll), (d) common-logarithm transformed nitrate concentration (log-nitrate), (e) latitude of the Kuroshio axis, and (f) common-logarithm transformed carbon-based diatom abundance (log-diatom). Diatom abundance data is available at only 10-m depth. The colors and shapes denote the areas and seasons, respectively (blue: coastal; green: offshore; closed circle: winter; open triangle: spring; cross: summer; closed square: autumn). The gray solid dashed line with shadow represents the linear regression line and 95% confidence values. When the linear regression line is the dashed line, the linear regression relationship is not significant ($p > 0.05$).

Figure 6. Responses of the least-AIC GLMs to $\delta^{13}C$ in terms of (a) temperature, (b) salinity, (c) log-chlorophyll, (d) log-nitrate, (e) latitude of the Kuroshio axis, and (f) log-diatom. Solid and dotted lines denote the GLMs of $\delta^{13}C$ fitting with the linear and quartic functions, respectively. Blue and green vertical ticks on the x-axes indicate the data points of the coastal and offshore areas, respectively. The numerical values of common-log transformed values (c, d, and f) are re-transformed to the normal values, but the axes are shown with the common-log transformed values.

Figure 7. Responses of the least-AIC GLMs to $\delta^{15}N$ in terms of (a) temperature, (b) salinity, (c) log-chlorophyll, (d) log-nitrate, (e) latitude of the Kuroshio axis, and (f) log-diatom. Solid and dotted lines denote the GLMs of $\delta^{15}N$ fitting with the linear and quartic functions, respectively. Blue and green vertical ticks on the x-axes indicate the data points of the coastal and offshore areas, respectively. The numerical values of common-log transformed values (c, d, and f) are re-transformed to the normal values, but the axes are shown with common-log transformed values. Gray horizontal lines denote that the parameter is not selected in the least-AIC GLMs.

Figure 8. Yearly variations in the least square means (lsmean, closed circle) of $\delta^{13}C$ (a, b) and $\delta^{15}N$ (c, d) based on the linear GLM (a, c) and quartic GLM (b, d). Vertical lines denote the 2 × standard errors (*i.e.*, 95% confidence intervals).

Figure 9. Scatter plot of the calculated climatological $\delta^{13}C$ and $\delta^{15}N$ values in each season and area based on the seasonal and spatial median values. The colors denote the seasons, and the shapes denote the combination of areas (open: offshore; closed: coastal) and models (square: linear function GLMs; circle: quartic function GLMs).

Figure 1.

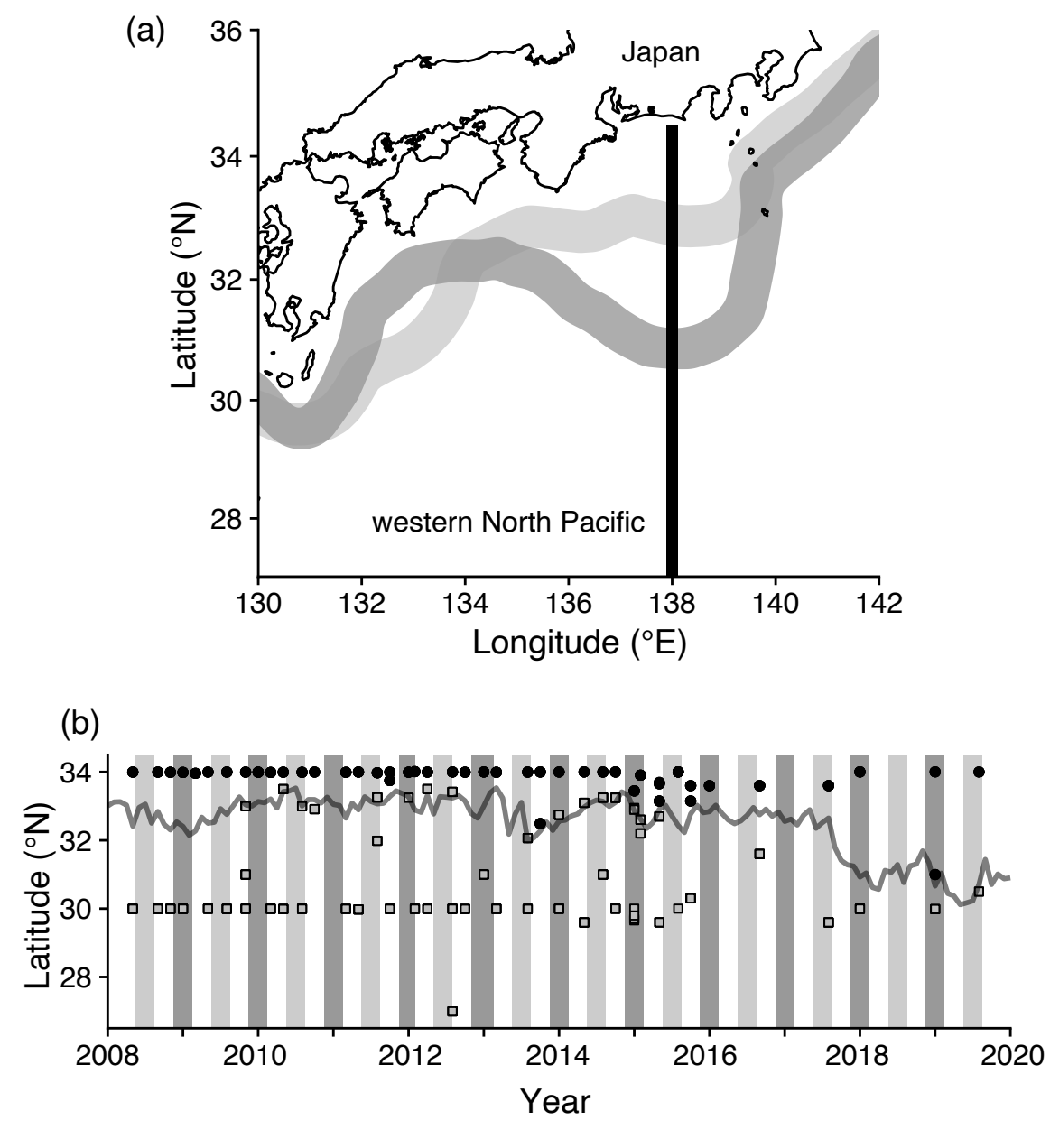
(a)
Japan
western North Pacific
Latitude (°N)
Longitude (°E)
36
34
32
30
28
130
132
134
136
138
140
142
(b)
Latitude (°N)
Year
34
32
30
28
2008
2010
2012
2014
2016
2018
2020

Figure 2.

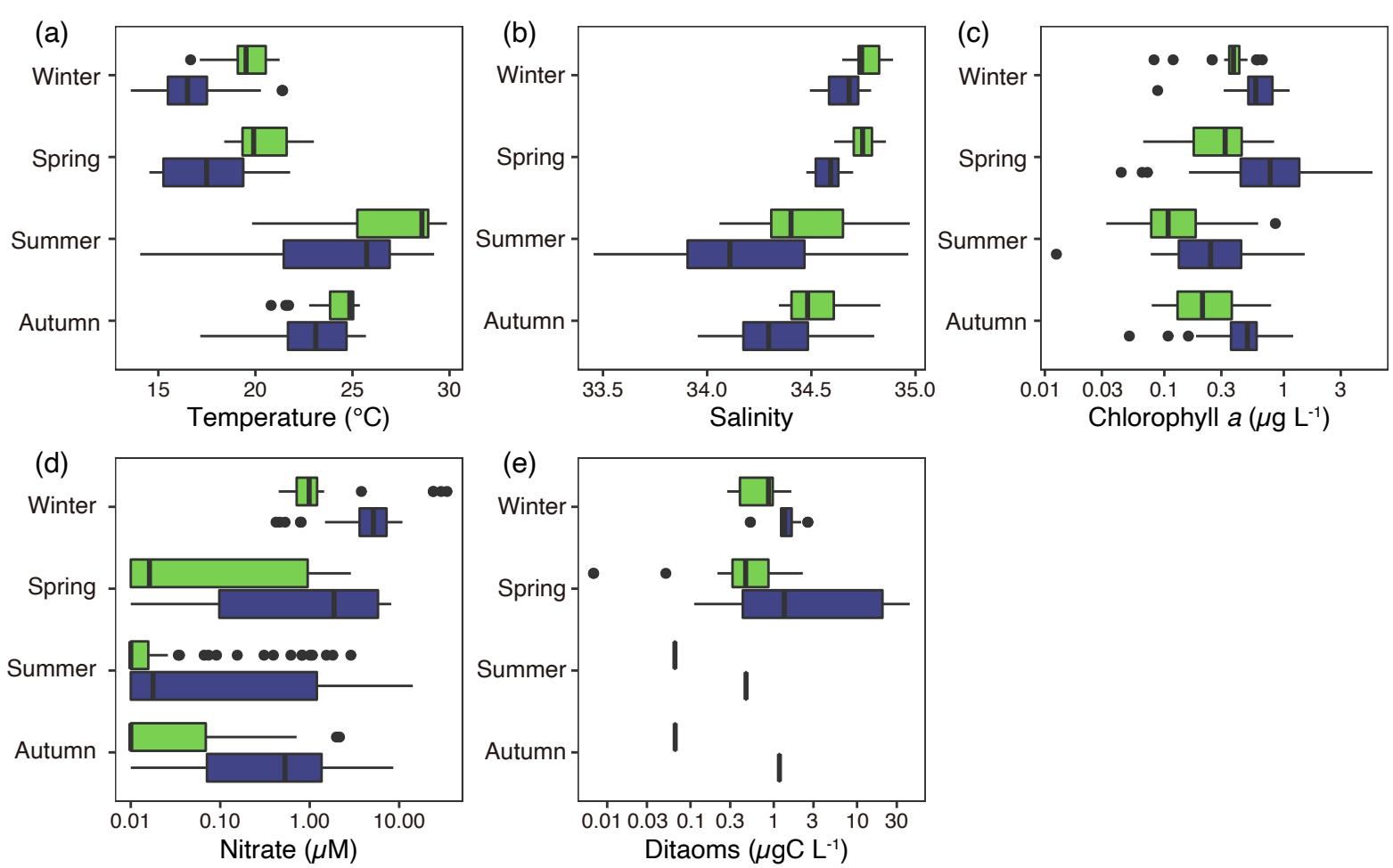
(a)
Winter
Spring
Summer
Autumn
15
20
25
30
Temperature (°C)
(b)
Winter
Spring
Summer
Autumn
33.5
34.0
34.5
35.0
Salinity
(c)
Winter
Spring
Summer
Autumn
0.01
0.03
0.1
0.3
1
3
Chlorophyll a (μg L-1)
(d)
Winter
Spring
Summer
Autumn
0.01
0.10
1.00
10.00
Nitrate (μM)
(e)
Winter
Spring
Summer
Autumn
0.01 0.03 0.1 0.3 1 3 10 30
Ditaoms (μgC L-1)

Figure 3.

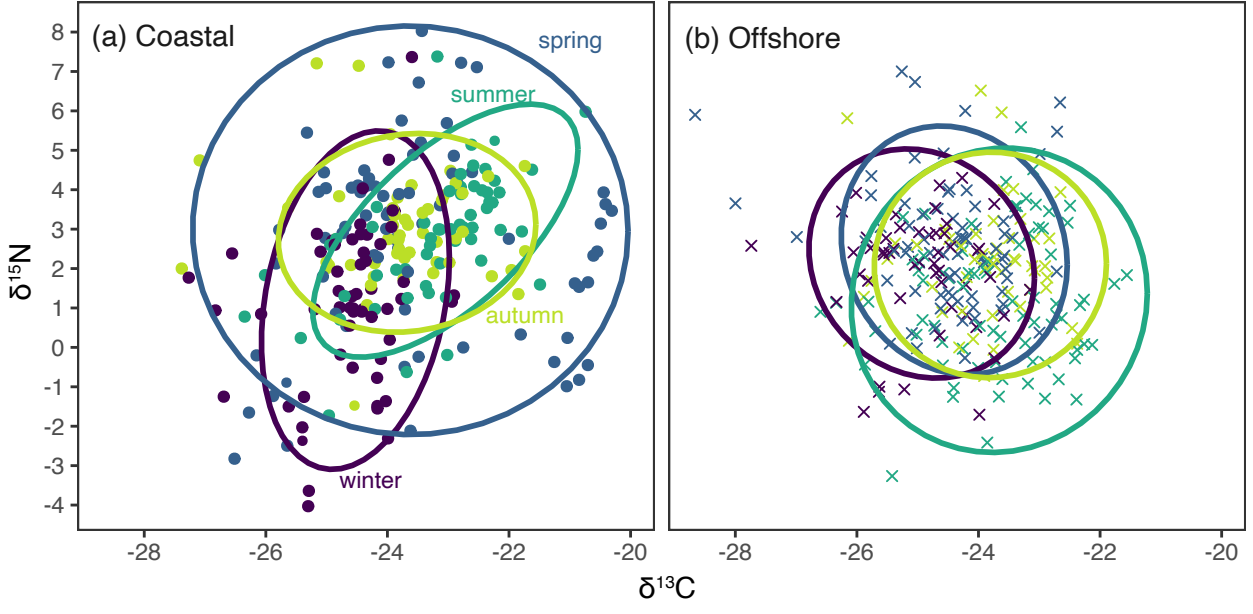
(a) Coastal
(b) Offshore
spring
summer
autumn
winter
δ15N
δ13C
8
7
6
5
4
3
2
1
0
-1
-2
-3
-4
-28
-26
-24
-22
-20

Figure 4.

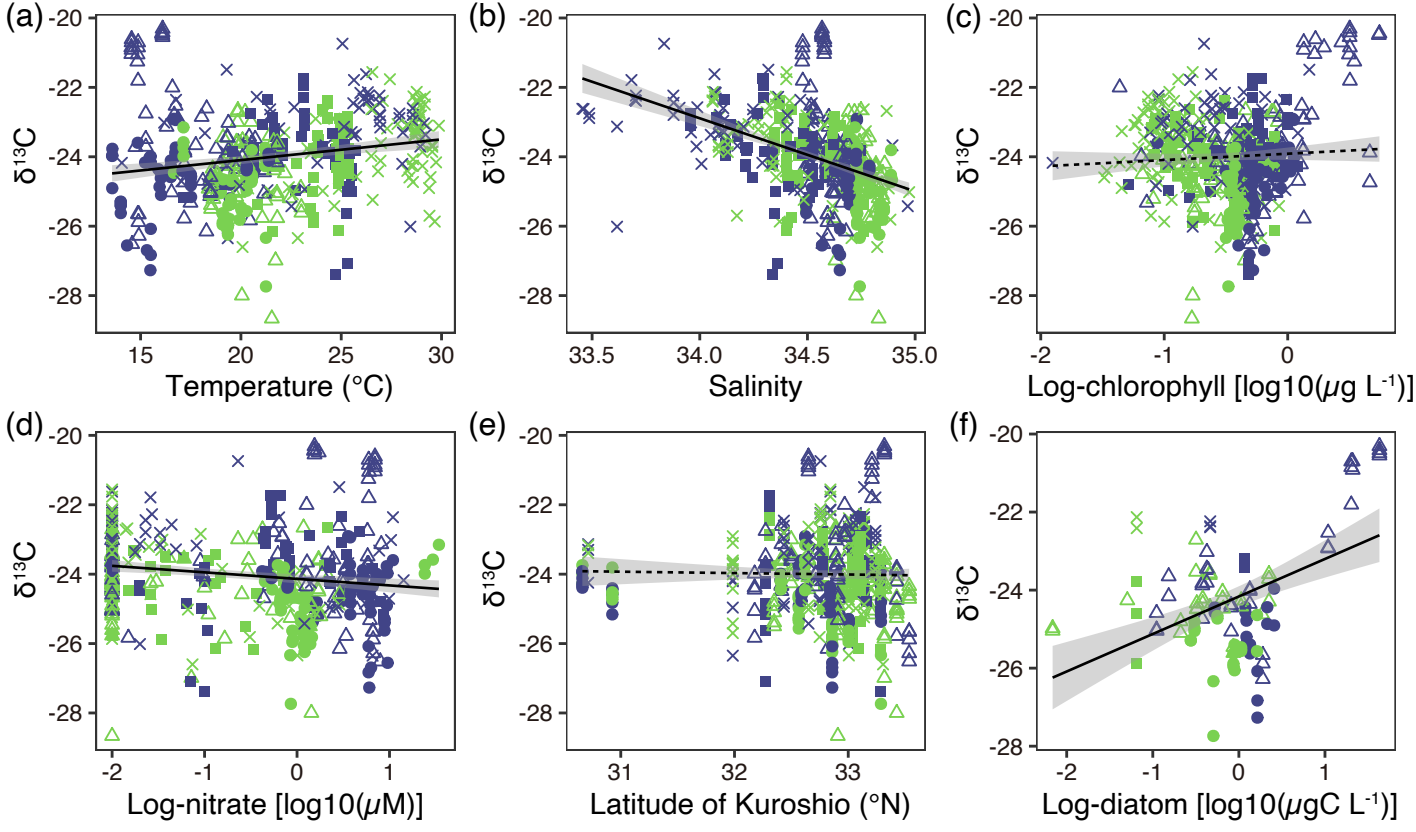
(a)
(b)
(c)
(d)
(e)
(f)
δ13C
-20
-22
-24
-26
-28
15
20
25
30
Temperature (°C)
33.5
34.0
34.5
35.0
Salinity
-2
-1
0
Log-chlorophyll [log10(μg L-1)]
1
Log-nitrate [log10(μM)]
31
32
33
Latitude of Kuroshio (°N)
Log-diatom [log10(μgC L-1)]

Figure 5.

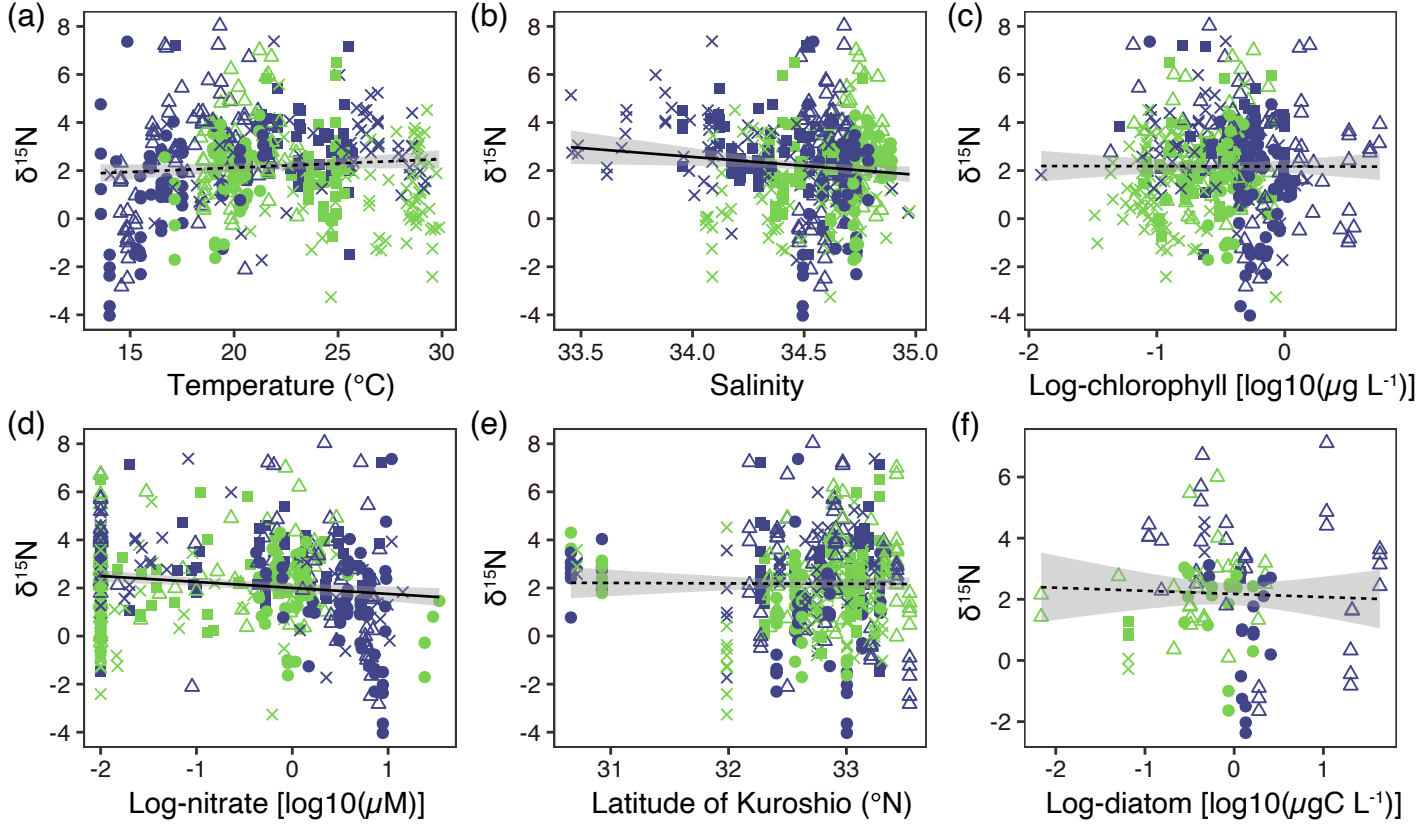
(a)
(b)
(c)
(d)
(e)
(f)
δ15N
Temperature (°C)
Salinity
Log-chlorophyll [log10(μg L-1)]
Log-nitrate [log10(μM)]
Latitude of Kuroshio (°N)
Log-diatom [log10(μgC L-1)]

Figure 6.

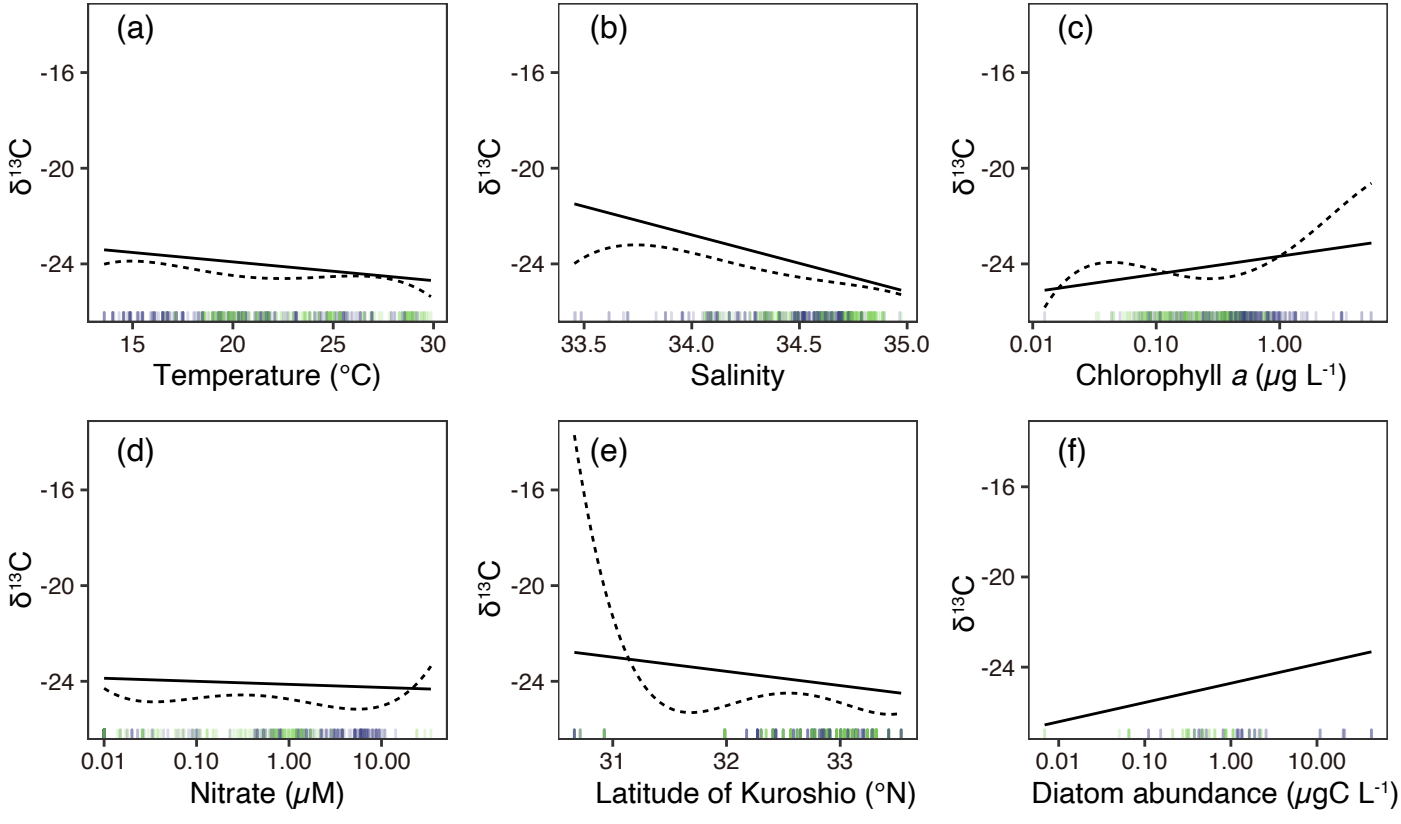
(a)
(b)
(c)
(d)
(e)
(f)
δ13C
-16
-20
-24
15
20
25
30
Temperature (°C)
33.5
34.0
34.5
35.0
Salinity
0.01
0.10
1.00
Chlorophyll a (μg L-1)
0.01
0.10
1.00
10.00
Nitrate (μM)
31
32
33
Latitude of Kuroshio (°N)
0.01
0.10
1.00
10.00
Diatom abundance (μgC L-1)

Figure 7.

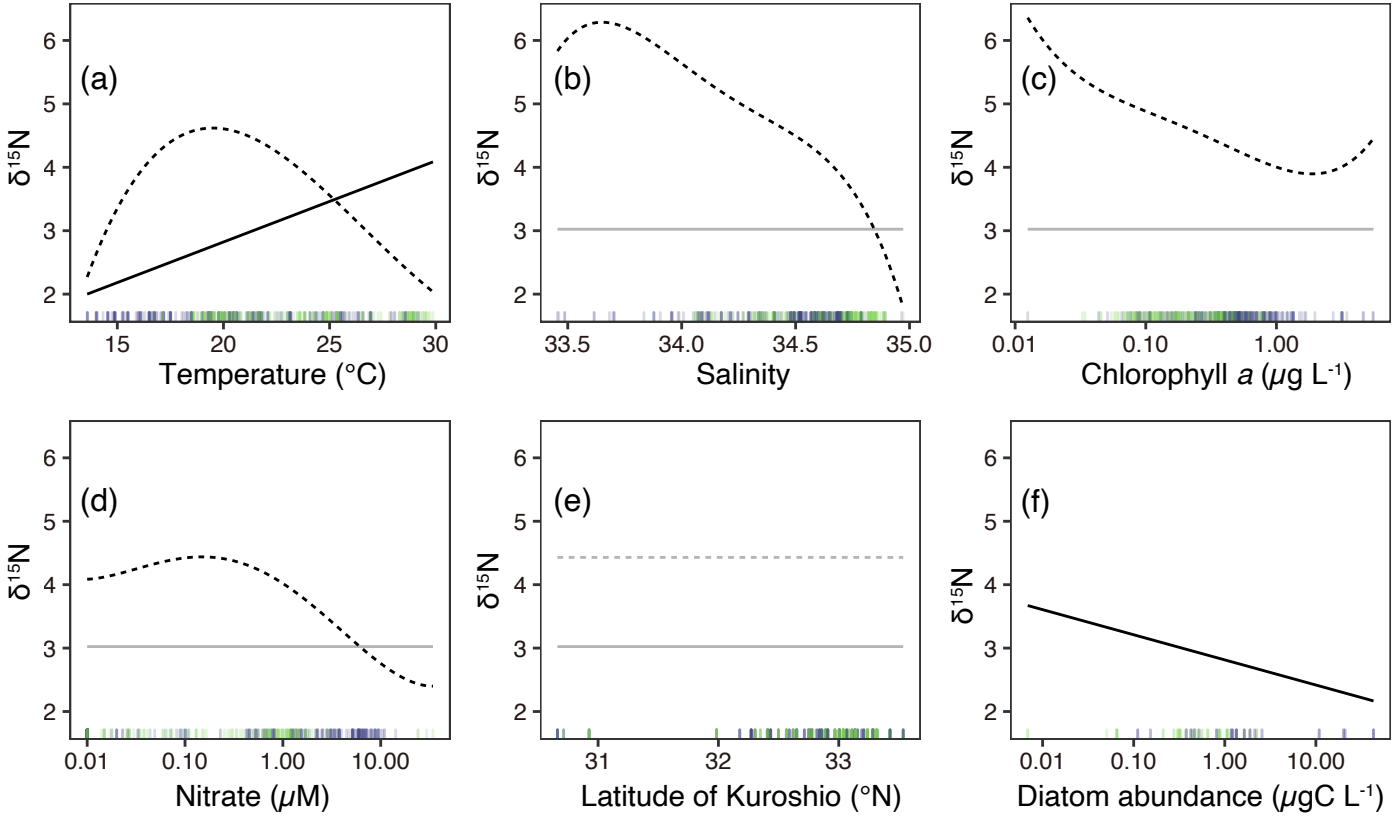
(a)
δ15N
Temperature (°C)
(b)
Salinity
(c)
Chlorophyll a (μg L-1)
(d)
Nitrate (μM)
(e)
Latitude of Kuroshio (°N)
(f)
Diatom abundance (μgC L-1)

Figure 8.

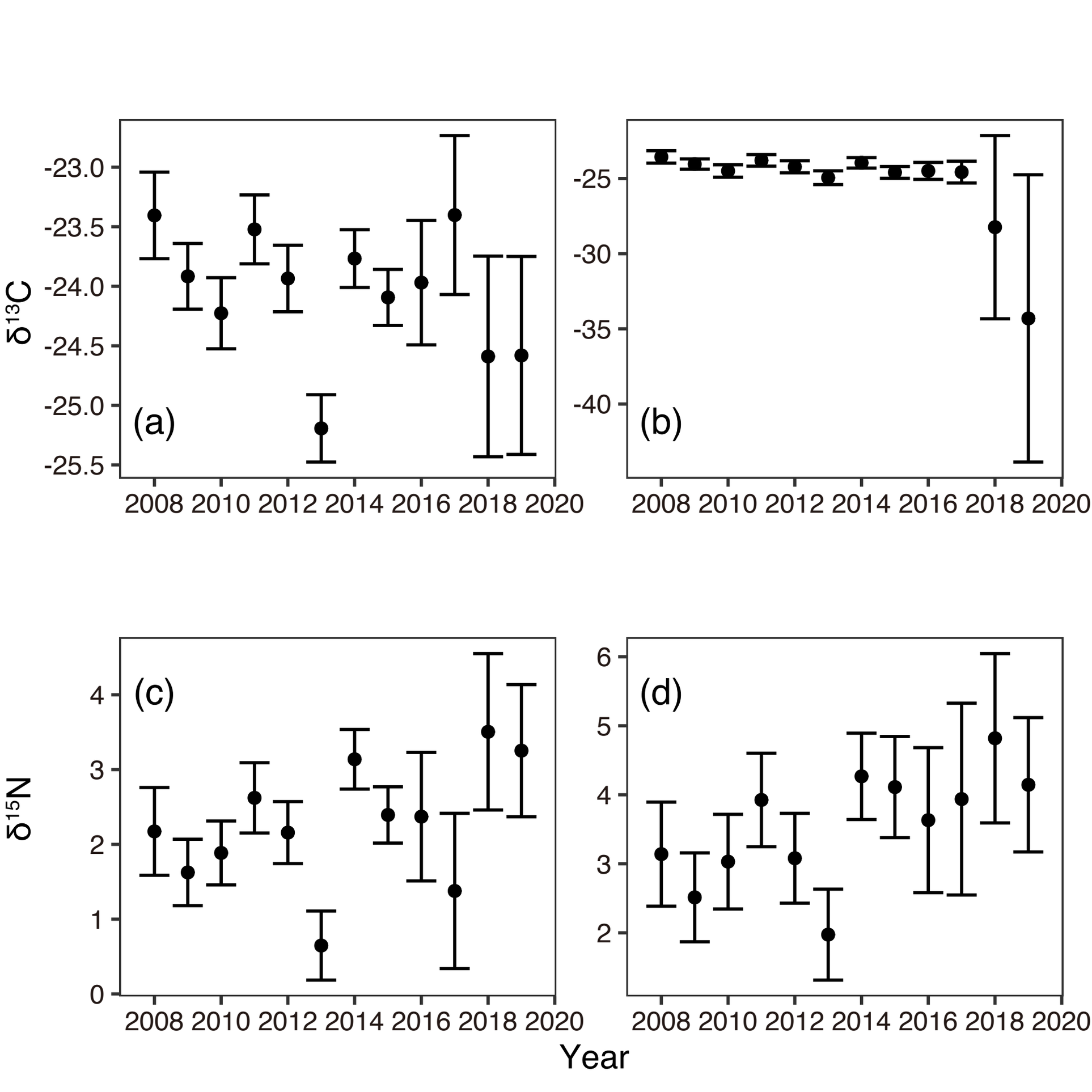
δ13C
δ15N
(a)
(b)
(c)
(d)
-23.0
-23.5
-24.0
-24.5
-25.0
-25.5
-25
-30
-35
-40
0
1
2
3
4
5
6
2008 2010 2012 2014 2016 2018 2020
Year

Figure 9.

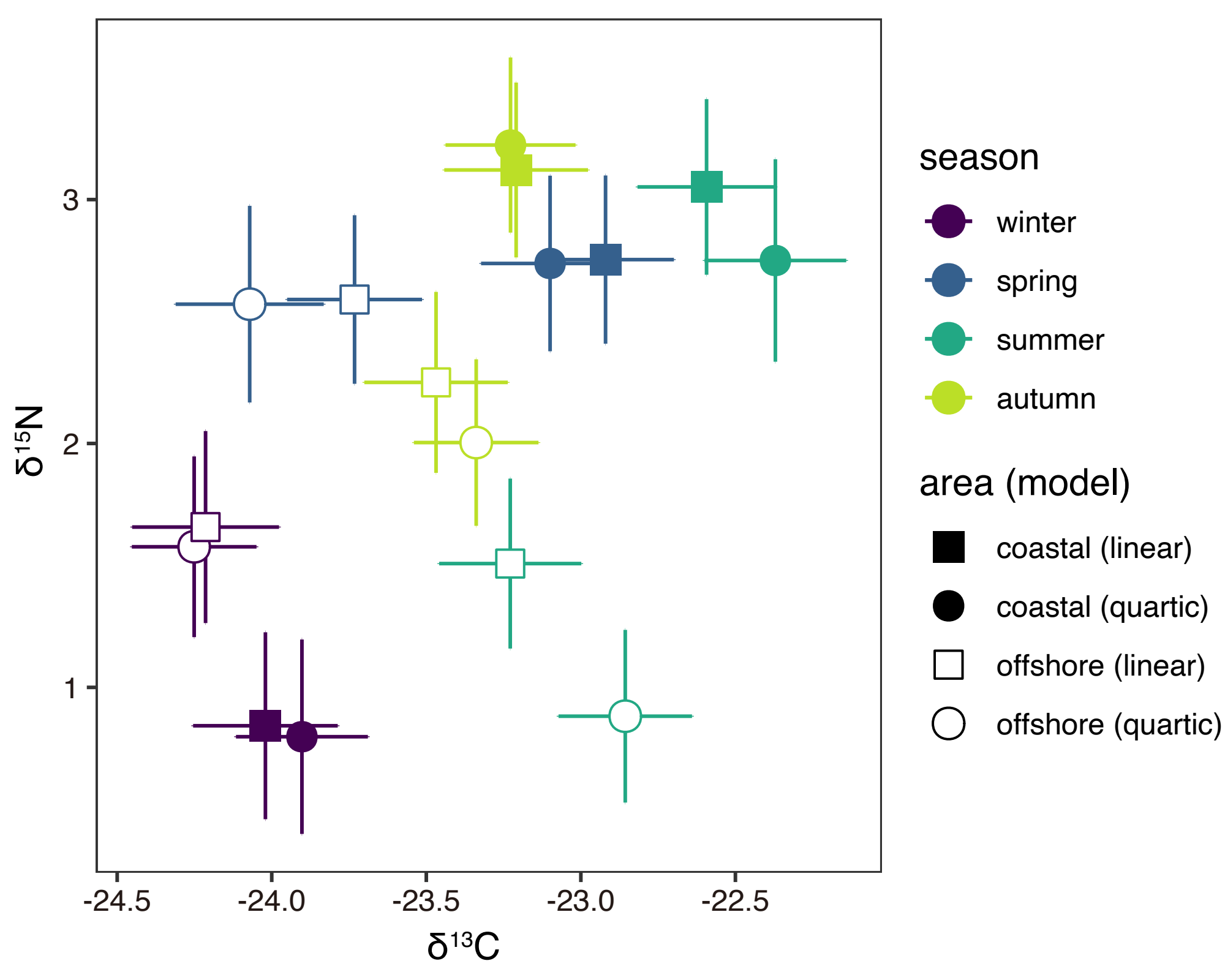
3
2
1
δ15N
-24.5
-24.0
-23.5
-23.0
-22.5
δ13C
season
winter
spring
summer
autumn
area (model)
coastal (linear)
coastal (quartic)
offshore (linear)
offshore (quartic)